# Brain-Based Biotypes of Psychiatric Vulnerability in the Acute Aftermath of Trauma

Jennifer S. Stevens, Ph.D., Nathaniel G. Harnett, Ph.D., Lauren A.M. Lebois, Ph.D., Sanne J.H. van Rooij, Ph.D., Timothy D. Ely, B.A., Alyssa Roeckner, B.S., Nico Vincent, B.S., Francesca L. Beaudoin, M.D., Ph.D., Xinming An, Ph.D., Donglin Zeng, Ph.D., Thomas C. Neylan, M.D., Gari D. Clifford, D.Phil., Sarah D. Linnstaedt, Ph.D., Laura T. Germine, Ph.D., Scott L. Rauch, M.D., Christopher Lewandowski, M.D., Alan B. Storrow, M.D., Phyllis L. Hendry, M.D., Sophia Sheikh, M.D., Paul I. Musey, Jr., M.D., John P. Haran, M.D., Ph.D., Christopher W. Jones, M.D., Brittany E. Punches, Ph.D., Michael S. Lyons, M.D., M.P.H., Michael C. Kurz, Meghan E. McGrath, M.D., Jose L. Pascual, M.D., Ph.D., Elizabeth M. Datner, M.D., Anna M. Chang, M.D., Claire Pearson, M.D., David A. Peak, M.D., Robert M. Domeier, M.D., Brian J. O'Neil, M.D., Niels K. Rathlev, M.D., Leon D. Sanchez, M.D., M.P.H., Robert H. Pietrzak, Ph.D., M.P.H., Jutta Joormann, Ph.D., Deanna M. Barch, Ph.D., Diego A. Pizzagalli, Ph.D., John F. Sheridan, Ph.D., Beatriz Luna, Ph.D., Steven E. Harte, Ph.D., James M. Elliott, Ph.D., Vishnu P. Murty, Ph.D., Tanja Jovanovic, Ph.D., Steven E. Bruce, Ph.D., Stacey L. House, M.D., Ph.D., Ronald C. Kessler, Ph.D., Karestan C. Koenen, Ph.D., Samuel A. McLean, M.D., M.P.H., Kerry J. Ressler, M.D., Ph.D.

**Objective:** Major negative life events, such as trauma exposure, can play a key role in igniting or exacerbating psychopathology. However, few disorders are diagnosed with respect to precipitating events, and the role of these events in the unfolding of new psychopathology is not well understood. The authors conducted a multisite transdiagnostic longitudinal study of trauma exposure and related mental health outcomes to identify neurobiological predictors of risk, resilience, and different symptom presentations.

**Methods:** A total of 146 participants (discovery cohort: N=69; internal replication cohort: N=77) were recruited from emergency departments within 72 hours of a trauma and followed for the next 6 months with a survey, MRI, and physiological assessments.

**Results:** Task-based functional MRI 2 weeks after a motor vehicle collision identified four clusters of individuals based on profiles of neural activity reflecting threat reactivity, reward reactivity, and inhibitory engagement. Three clusters were replicated in an independent sample with a variety of trauma types. The clusters showed different longitudinal patterns of posttrauma symptoms.

**Conclusions:** These findings provide a novel characterization of heterogeneous stress responses shortly after trauma exposure, identifying potential neuroimaging-based biotypes of trauma resilience and psychopathology.

*Am J Psychiatry 2021; 178:1037–1049; doi: 10.1176/appi.ajp.2021.20101526*

The diathesis-stress model of psychopathology has remained one of the most well-supported theories addressing the causes of mental disorders. In combination with predisposing factors, antecedent stressors increase risk for the onset and recurrence of depression (1), schizophrenia (2), insomnia (3), and posttraumatic stress disorder (PTSD) (4). However, stress and its severity or chronicity alone cannot account for the wide variety of different types of mental health outcomes that can follow major stressful life events (5), theoretically driven by existing individual differences (6). These variations and their biological bases are not well captured by existing definitions of psychiatric disorders. In the present study, our objective was to discover brain-based profiles to map heterogeneity following a stressor in a nationwide longitudinal study of trauma exposure and subsequent mental health outcomes, the Advancing Understanding of Recovery After Trauma (AURORA) study (7).

Neuroimaging is an attractive tool for mapping symptoms to biology. Previous efforts to account for heterogeneity have often explored brain-wide patterns of activation or connectivity to identify "biotypes," subtypes of a particular form of psychopathology that differ in their neurophysiological

*See related feature:* **Editorial** *by Dr. Knight (p. 991)*

features (8–10). The identification of such subgroups may in turn improve our understanding of variance in outcomes and response to treatment. However, previous work has defined the neuroimaging features of interest on the basis of their association with either a specific symptom type or the response to treatment. These backward inferences constrain the solution to features that already have high relevance to a diagnostic category, potentially excluding features that contribute to atypical symptom profiles and raising concerns related to overfitting (11). Taking a complementary approach, we constructed a forward inference model, examining neuroimaging profiles in the acute posttrauma period and then investigating their association with the emergence of later symptoms. The goal was to identify posttrauma biotypes with relevance to overall stress vulnerability and resilience but not specific to a particular diagnosis or symptom.

Neural models of stress vulnerability involve hyperreactivity of regions involved in threat detection and the fear response, such as the amygdala, insula, and dorsal anterior cingulate cortex (dACC) (12–15). In addition, both chronic depression and PTSD emerging following a stressful event appear to be preceded by low reward reactivity in affective-evaluative regions, including the nucleus accumbens (NAcc), amygdala, and orbitofrontal cortex (OFC) (16–20). Finally, reduced pretrauma or early posttrauma engagement of regions involved in inhibition, including the ventromedial prefrontal cortex (vmPFC) and hippocampus, is also predictive of greater subsequent PTSD and lower resilience (12, 21–24). Therefore, an early posttrauma profile of co-occurring high threat reactivity, low reward reactivity, and low inhibition would likely be predictive of later chronic symptoms of PTSD and depression. However, it is not yet clear whether these features co-occur within particular individuals or groups. Building a brain-based model of individual differences in the response to major stressors is critical for efforts to construct effective intervention and prevention strategies for stress-related psychiatric disorders.

Here, we collected functional MRI (fMRI) scans in a regionally diverse cohort of civilian trauma survivors 2 weeks posttrauma (7). Participants reported on symptoms of psychopathology through mobile surveys over the first 6 months posttrauma. fMRI-based phenotypes used in the biotyping analysis were motivated by previous longitudinal studies of stress exposure and included all brain regions previously linked with vulnerability to poststress psychopathology within the domains of threat responsivity, reward responsivity, and inhibition/impulsivity as described above. Participants engaged in fMRI tasks that were simple in their design and interpretation and that have been widely used to probe threat (12), reward (25), and response inhibition (26). Multivariate profiles of regional activation were entered into a hierarchical clustering analysis to identify brain-based groupings of individuals in the early posttrauma period, indicative of distinct biotypes. We predicted that fMRI-based clusters would be associated with different patterns of subsequent posttrauma symptoms across PTSD, dissociation, anxiety, depression, and impulsivity. Finally, to better understand whether the clusters overlap with widely known biomarkers of chronic posttraumatic pathology, such as deficits in fear inhibition (27) and extinction (28), we tested whether the clusters differed in these features in a fear-potentiated startle paradigm conducted on the same day as the fMRI scan.

## METHODS

### Participants

Participants were recruited from emergency departments as part of a multisite longitudinal study of adverse neuropsychiatric sequelae of trauma (7). Twenty-two emergency departments within the Northeast, Southern, Mid-Atlantic, and Midwest regions of the United States enrolled patients within 72 hours of trauma exposure. All participants were ages 18–75, able to speak and read English, oriented to time and place, and physically able to use a smartphone, and they had possessed a smartphone for more than 1 year. Potential participants were excluded if they had a solid organ injury greater than grade 1 or a significant hemorrhage, required a chest tube or general anesthesia, or were likely to be admitted for >72 hours. MRI scans and psychophysiology data were collected a mean of 18 days (SD=6) later at a laboratory visit at McLean Hospital (Belmont, Mass.), Emory University (Atlanta), Temple University (Philadelphia), or Wayne State University (Detroit), which were each located in proximity to multiple enrolling sites. Written informed consent was obtained as approved by each site's institutional review board.

Data collection for the AURORA study is ongoing. The discovery cohort included an initial sample that was restricted to motor vehicle-related traumas for participants with at least 8 weeks of follow-up data by March 2019 (94 patients completed the MRI visit). Data for the replication cohort were separate from the discovery cohort because these data had not yet been released by the time of the initial analysis. A second freeze and release of the survey data was broadened to include all trauma types with at least 8 weeks of follow-up data by mid-October 2019. Unique participants in this second freeze made up the replication cohort (additional participants, N=108). After quality control, 69 participants in the discovery cohort and 77 in the replication cohort were retained for analyses. The study participants' demographic characteristics are presented in Table 1.

### Demographic Variables and Psychiatric Assessment

Trauma severity was measured using an injury severity score, as well as participants' subjective ratings of their chances of dying. Assessments of pretrauma risk factors included a general physical health status assessment, childhood maltreatment assessment, and demographic variables. Assessments of posttrauma outcomes, including PTSD symptoms, depression symptoms, dissociative symptoms, anxiety symptoms, and impulsivity, were assessed for the pretrauma period (queried in the emergency department) and at 2 weeks (days 7–21),

8 weeks (days 46–67), 3 months (days 77–104), and 6 months (days 168–195) posttrauma. Measures and scoring details are summarized in the online supplement.

**TABLE 1. Demographic and trauma-related characteristics of trauma survivors in the Advancing Understanding of Recovery After Trauma study**

| | Cohort | | | | | |
|---|---|---|---|---|---|---|
| | Discovery (N=69) | | Replication (N=77) | | Group Comparison | |
| Characteristic | N | % | N | % | $\chi^2$ | p |
| Site | | | | | 1.81 | 0.61 |
| 1 | 5 | 7.2 | 2 | 2.6 | | |
| 2 | 28 | 40.7 | 32 | 41.6 | | |
| 3 | 19 | 27.5 | 24 | 31.2 | | |
| 4 | 17 | 24.6 | 19 | 24.7 | | |
| Female | 51 | 73.9 | 48 | 62.3 | 2.23 | 0.14 |
| Race/ethnicity | | | | | 6.62 | 0.09 |
| Hispanic/Latino | 11 | 15.9 | 12 | 15.6 | | |
| White | 20 | 29.0 | 34 | 44.2 | | |
| Black/African American | 37 | 53.6 | 27 | 35.1 | | |
| Asian, Hawaiian, American Indian, or other | 1 | 1.4 | 4 | 5.2 | | |
| Education | | | | | 20.02 | 0.05 |
| Less than high school | 3 | 4.3 | 3 | 3.9 | | |
| High school diploma/GED | 26 | 37.7 | 16 | 20.8 | | |
| Some college/associate's degree | 29 | 42.0 | 29 | 37.6 | | |
| Bachelor's degree | 8 | 11.6 | 19 | 24.7 | | |
| Master's degree | 3 | 4.3 | 8 | 10.4 | | |
| Doctorate | 0 | 0.0 | 2 | 2.6 | | |
| Employment status | | | | | 2.15 | 0.71 |
| Employed | 48 | 69.6 | 48 | 62.3 | | |
| Retired | 1 | 1.4 | 3 | 3.9 | | |
| Homemaker | 1 | 1.4 | 1 | 1.3 | | |
| Student | 2 | 2.9 | 4 | 5.2 | | |
| Unemployed, disabled, or other | 9 | 13.0 | 14 | 18.2 | | |
| Data missing | 8 | 11.6 | 7 | 9.1 | | |
| Yearly family income | | | | | 4.49 | 0.48 |
| <$19,000 | 17 | 24.6 | 17 | 22.1 | | |
| $19,001–$35,000 | 18 | 26.1 | 19 | 24.7 | | |
| $35,001–$50,000 | 10 | 14.5 | 13 | 16.9 | | |
| $50,001–$75,000 | 4 | 5.8 | 9 | 11.7 | | |
| $75,001–$100,000 | 3 | 4.3 | 7 | 9.1 | | |
| >$100,000 | 9 | 13.0 | 5 | 6.5 | | |
| Data missing | 8 | 11.6 | 7 | 9.1 | | |
| Trauma type | | | | | 42.82 | $9.51 \times 10^{-7}$ |
| Motor vehicle collision | 69 | 100.0 | 41 | 53.2 | | |
| Physical assault | 0 | 0.0 | 15 | 19.5 | | |
| Sexual assault | 0 | 0.0 | 2 | 2.6 | | |
| Incident causing traumatic stress exposure to many people | 0 | 0.0 | 1 | 1.3 | | |
| Nonmotorized collision (e.g., bicycle, skateboard) | 0 | 0.0 | 6 | 7.8 | | |
| Fall <10 feet | 0 | 0.0 | 4 | 5.2 | | |
| Burn | 0 | 0.0 | 1 | 1.3 | | |
| Animal-related | 0 | 0.0 | 3 | 3.9 | | |
| Other | 0 | 0.0 | 4 | 5.2 | | |
| | Mean | SD | Mean | SD | t | p |
| Age (years) | 33.6 | 12.1 | 35.3 | 13.7 | −0.80 | 0.42 |
| Injury severity scale | 2.5 | 2.4 | 2.3 | 1.8 | 0.80 | 0.42 |
| Patient-rated chance of dying | 5.6 | 3.6 | 4.8 | 3.3 | 1.48 | 0.14 |

## MRI

*Acquisition.* Brain imaging data were acquired on four separate Siemens 3-T MRI scanners using the two-dimensional echo-planar blood-oxygen-level-dependent sequence for functional scans and a magnetization-prepared rapid acquisition gradient echo $T_1$-weighted image for structural scans. Site-specific sequence parameters are presented in Table S5 in the online supplement.

*fMRI tasks.* The three fMRI tasks (Figure 1) included a threat task designed to probe reactivity to social threat cues (12), an inhibition task, which was a modified version of Liebenluft's stop-signal task (26), and a reward task, which was a short version of Delgado's monetary reward task (25).

*Preprocessing and analysis.* Full preprocessing information is reported in the online supplement. Functional images were preprocessed with fMRIPrep, version 1.2.2 (29). Echo-planar imaging scans were coregistered to the $T_1$-weighted images, then spatially realigned, slice-time corrected, and normalized to the 2009 ICBM-152 template. Volume-wise motion and other sources of artifact were corrected using ICA-AROMA (30). To handle cases in which motion was likely too high for effective independent component analysis correction, we also implemented an overall motion threshold for any run with >15% of volumes showing ≥1-mm framewise displacement. Images were then smoothed with a 6-mm kernel. Site-by-site quality metrics are plotted in Figure S3 in the online supplement.

The final sample was restricted to participants with good-quality data across all three fMRI tasks (threat, inhibition, and reward). We did not interpolate any data point because the goal of the clustering analysis was to identify existing

**FIGURE 1. Functional MRI scans during threat, inhibition, and reward tasks among trauma survivors in the Advancing Understanding of Recovery After Trauma study**[a]

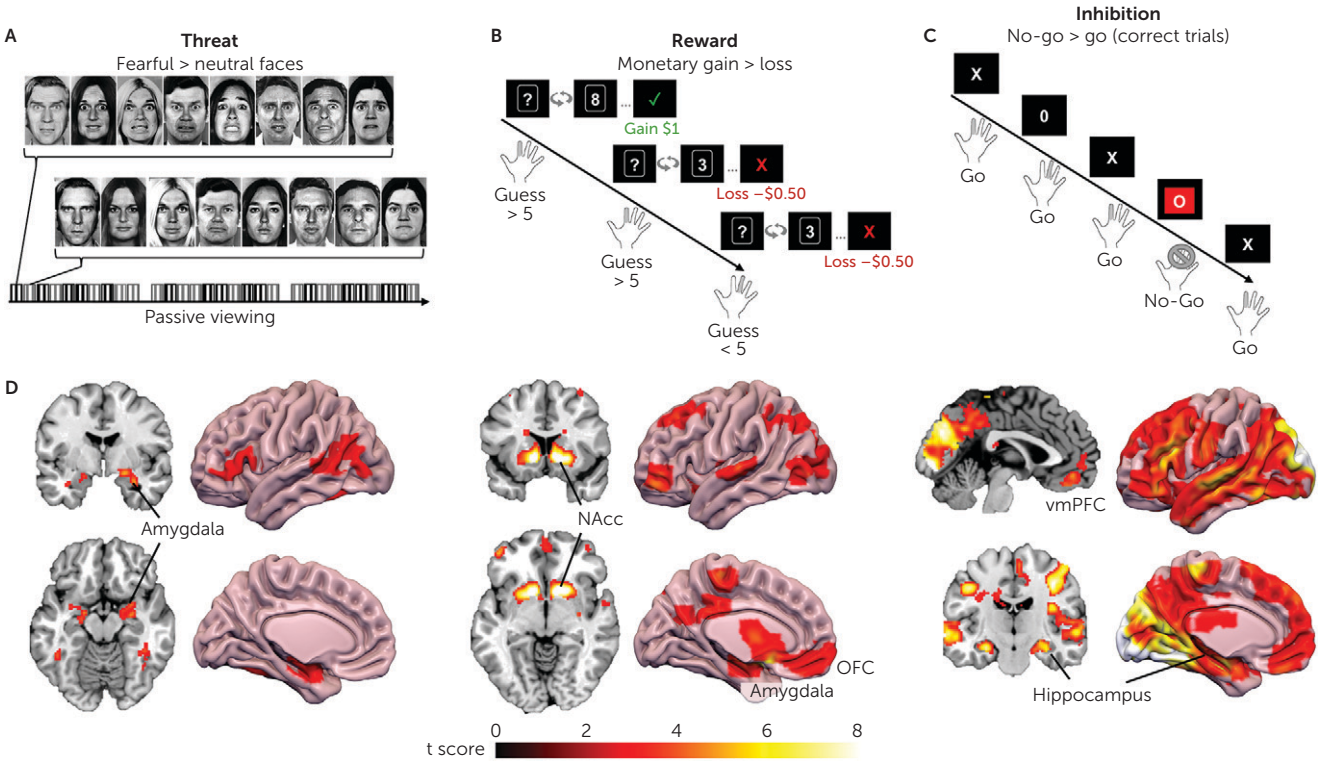


[a] In the threat task (panel A), participants passively viewed blocks of static fearful and neutral facial expressions. Each block contained eight different face stimuli, and the emotion condition of the blocks varied in a pseudorandom manner, with 15 fearful and 15 neutral blocks. Block order was counterbalanced across participants. Within each 8,000-ms block, faces were presented for 500 ms each, with a 500-ms interstimulus interval. Rest periods of 10,000 ms occurred after every 10 blocks, and participants were instructed to relax with their eyes open. In the reward task (panel B), participants viewed a card with a question mark and made a button press to indicate their guess about whether the card's value would be higher or lower than $5 when the card was "flipped over" to reveal its value. Participants were informed that they would win real money ($1) for each correct guess and lose $0.50 for each incorrect guess. There were 40 trials, each consisting of a guessing period of 2,000 ms, during which time the button press was recorded, followed by a short delay of 2,000–4,000 ms and then the display of the card's value and monetary outcome (a green check indicating gain and a red X indicating loss). Unknown to participants, the outcome of each card guess was predetermined to create 20 gain trials and 20 loss trials, and participants always won $10. In the inhibition task (panel C), participants were presented with a series of X's or O's that required a rapid behavioral response (X=index finger press; O=middle finger press) and were asked to inhibit this response on trials that included a red background, the stop signal. There were four runs of 26 go trials, 13 no-go trials, and 14 blank trials (black background only), randomly ordered. Trials consisted of either the X or the O displayed for 1,000 ms, and on no-go trials, a red rectangle appeared behind the X or O, and participants were asked to withhold all responses. Trials were followed by a jittered intertrial interval of 1,250–2,500 ms and a 500-ms fixation cross. Brain images show task-responsive voxels for the key contrast of interest (panel D) in a whole-brain analysis across all participants (N=146) (false discovery rate corrected $p<0.05$). NAcc=nucleus accumbens; OFC=orbitofrontal cortex; vmPFC=ventromedial prefrontal cortex.

patterns of activation across the three tasks. Participants were excluded for falx calcification (discovery cohort, N=0; replication cohort, N=5); discontinuing the scan before completing all three tasks (discovery cohort, N=4; replication cohort, N=7); superthreshold head motion on one or more tasks (discovery cohort, N=11; replication cohort, N=5); technical reasons, such as problems with stimulus display on one or more tasks (discovery cohort, N=2; replication cohort, N=4); or low behavioral performance on either the inhibition or reward task (<75% of trials receiving a button press, indicating sleepiness or low effort; discovery cohort, N=8; replication cohort, N=8). The analysis therefore included 69 participants in the discovery cohort and 77 in the replication cohort.

Statistical modeling of the fMRI data and region of interest definitions are detailed in the online supplement. Regions of interest were defined anatomically and included the left and right amygdala, insula, subgenual anterior cingulate cortex (sgACC), dACC (threat: fearful > neutral faces), nucleus accumbens (NAcc), OFC, amygdala (reward: monetary gain > loss), hippocampus, and vmPFC (inhibition: no-go < go).

*Fear-potentiated startle.* Participants completed fear-acquisition and extinction tasks on the same day as the MRI scan. Details on the data acquisition and paradigm are presented in the online supplement.

### Clustering Analysis

Analyses were conducted in R, version 3.6.3, with RStudio, version 1.2.1335. All tests were two-tailed and used a significance threshold of 0.05, with family-wise error correction as noted in the Results section. Clustering was conducted on data from the regions of interest extracted from the three fMRI tasks, using hierarchical agglomerated clustering, with the *cluster* package, version 2.1.0, following Ward's criterion (agnes function). This is a bottom-up method designed to preserve the existing structure of the data without imposing assumptions of linearity, appropriate for exploratory analysis. The optimal number of clusters was determined using silhouette (31) and distance (32) methods. Nonparametric bootstrapping using the *fpc* package, version 2.2.5, was applied to the cluster solutions, with 1,000 iterations. After the initial hierarchical clustering, the data were randomly resampled with replacement. In each bootstrap, clustering was performed on the resampled data, and the new cluster most similar to each original cluster was identified by saving the maximum Jaccard coefficient (indexing similarity) for each old-new comparison (33). This was repeated, and a mean permuted Jaccard coefficient was computed across all the bootstraps by cluster. Permuted Jaccard coefficient therefore represents the proportion of individuals from each original cluster solution that were again clustered together in the permuted data. A permuted Jaccard coefficient of 0.6–0.75 indicates stable clusters, >0.75 represents high stability, and <0.50 is thought to indicate cluster instability (33); clusters were considered reconstituted on any bootstrap with a permuted Jaccard coefficient >0.60.

The replication was assessed quantitatively using a train and test approach. We trained a simple k-nearest-neighbors (knn function) model (34) with the *class*, version 7.3, package using the discovery cohort data, labeled using the cluster labels from the hierarchical clustering solution. We applied this knn model ("test") in the replication cohort to obtain a new set of labels. We then compared these new labels to the de novo hierarchical clustering of the replication cohort in *caret*, version 6.0 (35).

### Analysis of Posttrauma Outcomes by Cluster

Because clustering produced some small cells within-cohort (Ns as low as 11), we combined the clusters that replicated between the discovery and replication cohorts for further characterization. Cluster assignments from the initial cluster solutions were retained, rather than reclustering in a combined data set.

Chi-square tests (categorical variables) or one-way analyses of variance (ANOVAs) (continuous variables) were used to assess whether demographic factors or trauma-related factors differed between the cluster groups.

Given the multiple overlapping adverse mental health outcomes of trauma, we used multivariate analysis of variance (MANOVA) to test whether the pattern of subsequent mental health outcomes varied across the cluster groups. The outcome was a vector of standardized scores for PTSD symptoms, depression symptoms, dissociation, anxiety, and impulsivity. Predictors included cluster, assessment time point (time-invariant term for the 2-week, 8-week, 3-month, and 6-month posttrauma assessments; linear and quadratic terms), cluster-by-time point interaction, cohort, and a random effect for participant. Post hoc tests separating each outcome type were conducted using linear mixed models in the *lme4* package, with the same set of predictors used in the MANOVA. To test whether the fMRI-based clustering provided incremental information above and beyond pretrauma symptom levels, we conducted secondary models including pretrauma symptoms that participants reported in the emergency department. Initial AURORA study findings indicated that among sociodemographic risk factors, pretrauma symptom levels were the strongest predictor of later PTSD and depression symptom severity (36, 37).

Finally, we tested whether a dimensional model of the 2-week fMRI data outperformed cluster assignment in predicting posttrauma outcomes using the first three principal components from the principal component analysis of the nine regions of interest in the combined discovery and replication data set as dimensional predictors of later outcomes. These models used the same structure as the cluster-based analyses. Model fit for dimensional and cluster-based models were directly compared.

Fear-potentiated startle during fear conditioning and extinction was also collected on the same day as the MRI scan (acquisition details are presented in the online supplement). ANOVAs tested whether the cluster groups varied in fear-potentiated startle responses during either acquisition or extinction as a function of cluster, cohort, block, and conditioned stimulus (CS) type and interactions between cluster, block, and CS type.

## RESULTS

### Covariance Among the fMRI Tasks and Regions of Interest

To assess for feature redundancy, we examined the covariance structure between the tasks and regions of interest. Regions of interest showed positive within-task covariance but not between tasks (Figure 2A,B). The small to moderate correlations suggested that each task and region would contribute unique variance to a clustering analysis. Interestingly, similar regions were uncorrelated from one task to another; for example, participants' amygdala reactivity to threat was not correlated with amygdala reactivity to reward ($r=0.00$, $p=0.97$). This suggests that the "crud" factor (everything correlates with everything) (38) was very low across this set of tasks.

### Clustering of Individuals Using Task-Based fMRI 2 Weeks Posttrauma

Hierarchical clustering was first applied in the discovery sample, with 69 survivors of motor vehicle accidents. A four-cluster solution was identified (Figure 2C; see also Figure S1A,B in the online supplement). Silhouette results

**FIGURE 2. Functional MRI (fMRI) profiles of four clusters among trauma survivors in the Advancing Understanding of Recovery After Trauma study in the discovery (N=69) and replication (N=77) cohorts[a]**

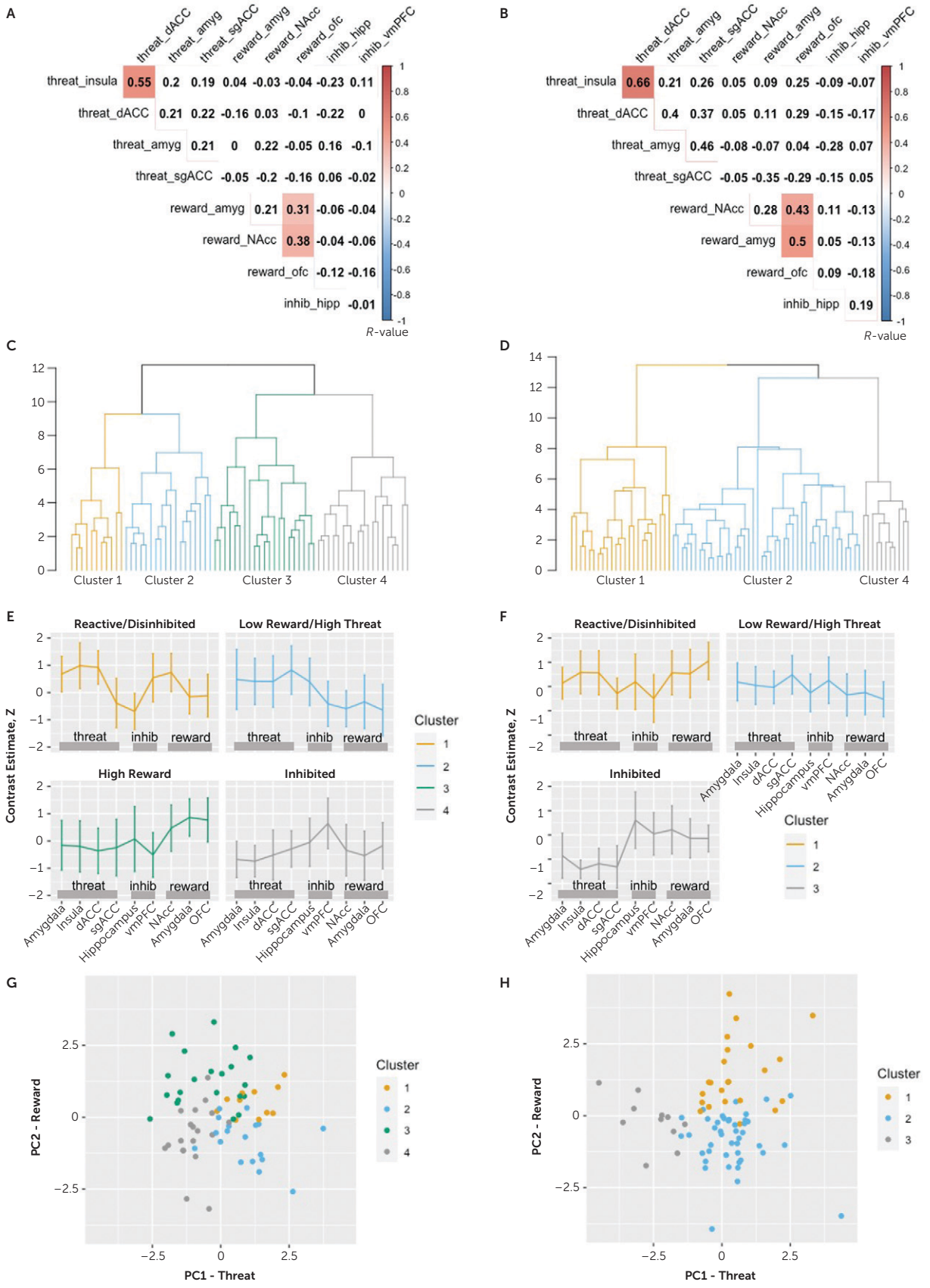

suggested an optimal clustering with two groups (k=2) but with only a small decrement in width for k=4, whereas Hartigan's distance metric showed an optimal gain in cluster cohesiveness at k=4. Examination of fMRI activation patterns (Figure 2E,G) indicated that individuals in cluster 1 (permuted Jaccard coefficient=0.52) showed high reactivity to both threat and reward, with little engagement of regulatory regions in threat or inhibition. Thus, we classified the cluster 1 group as "reactive/disinhibited." Individuals in cluster 2 (permuted Jaccard coefficient=0.54) showed threat responsivity predominated by the sgACC but low reward reactivity, and we classified this group as "low reward/high threat." Individuals in cluster 3 (permuted Jaccard coefficient=0.52) showed no reactivity to threat, nor engagement of the vmPFC or hippocampus during inhibition, but very high responsivity to reward, and we classified this group as "high reward." Finally, individuals in cluster 4 (permuted Jaccard coefficient=0.56) showed marked deactivation to threat in the amygdala, dACC, and insula, some activation of the hippocampus in the inhibition task, and little reactivity to reward, and we classified this group as "inhibited."

The replication cohort included 77 participants with a variety of different trauma types, including interpersonal traumas. Here, the most favorable clustering solution included three groups, with agreement between the silhouette and distance metrics at k=3 (Figure 2D; see also Figure S1C and D in the online supplement). The groups appeared to be consistent with cluster 1 (reactive/disinhibited; permuted Jaccard coefficient=0.53), cluster 2 (low reward/high threat; permuted Jaccard coefficient=0.73), and cluster 4 (inhibited; permuted Jaccard coefficient=0.55) from the discovery sample (Figure 2F,H). There was a striking absence of a high reward-like phenotype; individuals who showed high reward reactivity also showed high threat reactivity.

The inclusion of higher-impact traumas may have pushed reward-responsive individuals toward higher threat reactivity. To test this, we combined both cohorts and examined effects of either injury severity or interpersonal violence on threat reactivity in the amygdala. Injury severity positively predicted amygdala reactivity ($F=4.58$, df=1, 144, $p=0.03$; see also Figure S2 in the online supplement), whereas interpersonal compared with noninterpersonal trauma did not ($p=0.61$). High reward was therefore likely subsumed under the reactive/disinhibited phenotype, related to higher-acuity traumas.

In the quantitative assessment of replication for clusters 1, 2, and 4, we assessed the extent to which a model trained on the clustering solution from the discovery cohort could predict the clustering solution within the replication cohort. The model trained on the discovery cohort data had 65.0% (95% CI=53.2, 75.5) accuracy in predicting the original hierarchical clustering-based labels in the replication cohort, compared with a 45.4% no-information rate ($p=0.0005$, kappa=0.45). This indicated that the clustering solution in the replication cohort could be recapitulated above and beyond chance levels using only the features of the discovery cohort solution.

The clusters were unrelated to demographic, health-related, trauma-related, or site-specific factors in follow-up testing (see the online supplement) and thus appeared to reflect covert neurocognitive features.

### Prospective Trajectories of Mental Health Among the Four Clusters

We next assessed trauma-related outcomes across the clusters in a combined sample of 125 individuals from the clusters that replicated across both cohorts (see Figure S3 in the online supplement). The clusters showed different multivariate symptom profiles posttrauma ($F=2.25$, df=2, 948, $p=0.013$) (Figure 3A). Although assessment time point was included as a factor in the model, there was no interaction of cluster by time point on the symptom profile ($p=0.82$). Follow-up tests were then performed for each symptom type separately. First, there was an effect of cluster on the longitudinal model of PTSD symptoms (Wald $\chi^2=6.47$, $p=0.039$), with the highest symptoms in the reactive/disinhibited cluster (Figure 3B). The effect of cluster was reduced when pretrauma PTSD symptoms were added as a predictor in the model (cluster effect: $\chi^2=5.10$, $p=0.078$; pretrauma PTSD severity effect: $\chi^2=20.19$, $p<0.001$).

Second, there was an effect of cluster on the longitudinal model of anxiety symptoms (Wald $\chi^2=6.23$, $p=0.044$) that was higher in the reactive/disinhibited cluster (Figure 3E). This effect held after including pretrauma anxiety symptoms as a predictor in the model (cluster effect: $\chi^2=6.07$, $p=0.048$; pretrauma anxiety severity effect: $\chi^2=72.37$, $p<0.001$), suggesting that cluster information provided

[a] Panels A and B show the region-of-interest covariance matrices revealing linear associations between z-scored contrast estimates extracted from the nine regions of interest across three tasks: threat, inhibition (inhib), and reward. For threat reactivity, participants passively viewed fearful and neutral face stimuli. For threat reactivity, fMRI activation was extracted from the amygdala (amyg), dorsal anterior cingulate cortex (dACC), insula, and subgenual anterior cingulate cortex (sgACC) for the contrast of fearful > neutral faces. For reward reactivity, activation was extracted from the amygdala, nucleus accumbens (NAcc), and orbitofrontal cortex (OFC) for the contrast of gain > loss trials. For response inhibition, activation was extracted from the hippocampus (hipp) and ventromedial prefrontal cortex (vmPFC) for the contrast of no-go > go trials. Matrices are ordered hierarchically, such that regions that are more strongly associated with one another are adjacent. Significant associations are indicated on a red and blue color scale, thresholded at a p value <0.05, uncorrected. Panels C and D show the dendrograms illustrating the final cluster solution with four clusters in the discovery cohort and three clusters in the replication cohort. Panels E and F show cluster differences (mean and standard deviation) for standardized contrast estimates extracted from the regions of interest across the threat (fearful > neutral faces), inhibition (no-go > go), and reward (gain > loss) contrasts. Panels G and H show individual subjects plotted along summary dimensions that reflect variance associated with primarily threat (principal component [PC] 1) and primarily reward (PC2); color reflects cluster assignment. Principal components were not used in the clustering analysis but are used in the graphs to illustrate graphically the cluster features and are described in further detail in Table S1 in the online supplement. Three-dimensional animated plots showing the inhibition dimension (PC3) are presented in Figure S5 in the online supplement.

**FIGURE 3. Future patterns of mental health and fear learning in the four cluster groups among trauma survivors in the Advancing Understanding of Recovery After Trauma study[a]**

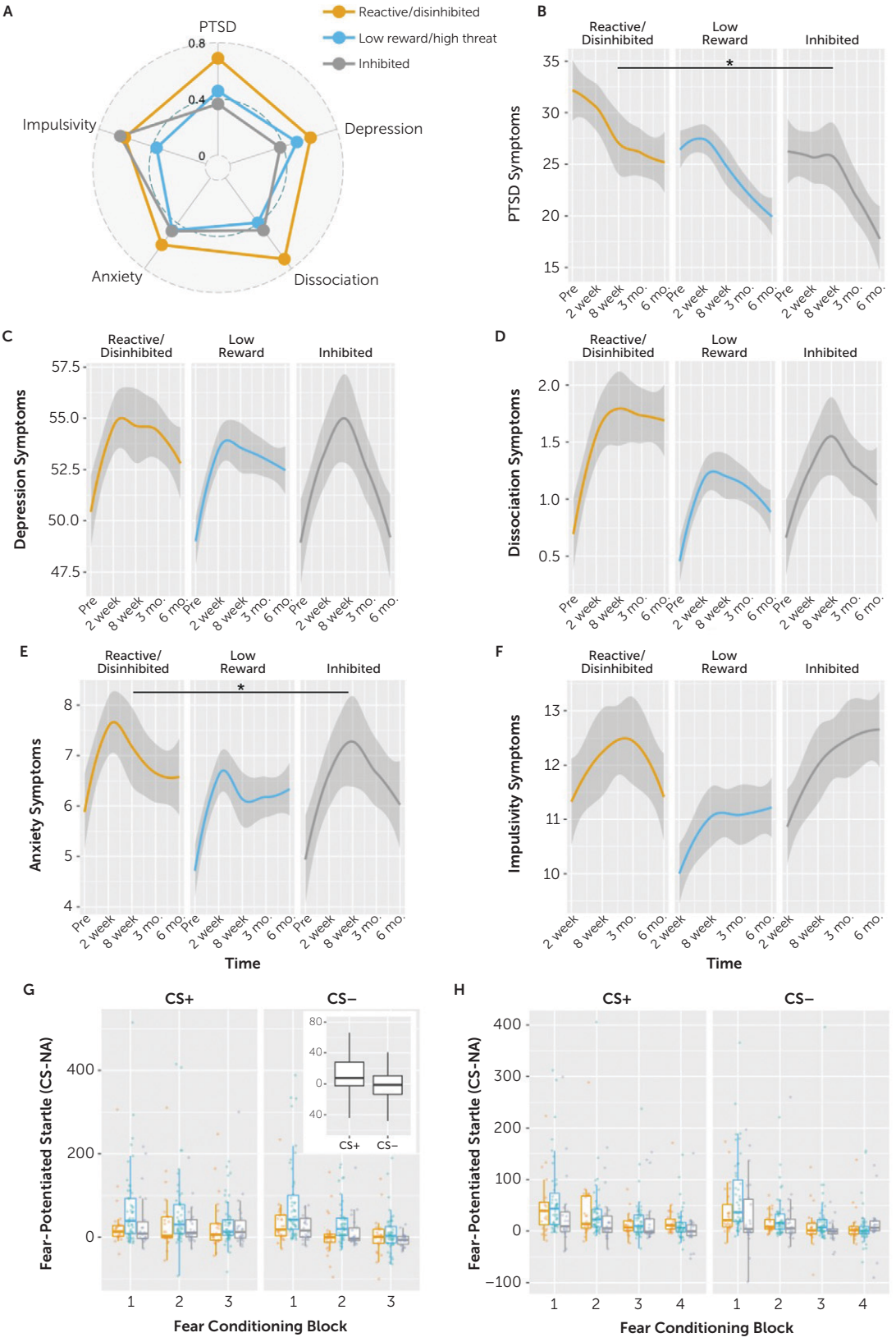

unique predictive value above baseline symptoms. Finally, cluster did not predict depressive (p=0.19) or dissociative symptoms (p=0.86) or impulsivity (p=0.96) (Figure 3C,D,F).

**Cluster-Based Compared With Dimensional Models for Predicting Longitudinal Posttrauma Outcomes**

We tested the utility of the discrete clusters against a dimensional model of the fMRI data for predicting longitudinal trajectories of stress-related symptoms. Dimensional fMRI predictors were continuous covariates reflecting threat reactivity, reward reactivity, and inhibition. Models with these covariates as predictors of later posttrauma symptoms showed negligible improvement in the model fit over the cluster-based models (see Table S3 in the online supplement). The individual fMRI dimensions were not linearly associated with any posttrauma outcome, with the exception of a negative association between the inhibition-related fMRI dimension and later dissociative symptoms (p=0.044). In models that included both clusters and dimensions competing for the variance in posttrauma outcomes, cluster assignment still predicted subsequent PTSD symptoms (p=0.012), whereas the three fMRI dimensions did not (all p values >0.05). For anxiety, neither cluster (p=0.080) nor dimensions (all p values >0.05) were significant in the head-to-head model. In summary, the dimensional model did not provide better predictive value than the cluster-based models.

**Convergent Validity With Fear-Learning Phenotypes**

On the day of the MRI scan, participants also completed a fear-potentiated startle paradigm that included fear conditioning and extinction. During fear conditioning, effects of CS (F=12.73, df=1, 468, p=0.0004) and the CS-by-block interaction (F=6.06, df=1, 468, p=0.003) suggested that fear conditioning occurred and that discrimination between the CS+ and CS− developed across acquisition. There was a significant cluster-by-block interaction (F=4.13, df=4, 468, p=0.003), such that the low reward/high threat cluster showed the highest fear-potentiated startle responses to both the CS+ and CS− at the beginning of fear conditioning, but this cluster was comparable to the other cluster groups by the end of the task (Figure 3G). There was no cluster-by-CS interaction (p=0.82). During fear extinction, startle responses to the CS+ and CS− showed the expected decline over time (block effect: F=28.79, df=3, 623, $p=0.02\times10^{-14}$), indicating the presence of extinction learning, but there was no interaction of CS by block (p=0.64), indicating no difference in the extinction pattern for CS+ compared with CS−. This was consistent with findings from previous studies of chronic PTSD using this startle paradigm (39). There was again an interaction of cluster by block, indicating different rates of extinction in the different cluster groups (F=2.35, df=6, 623, p=0.03). The low reward/high threat cluster showed the highest fear-potentiated startle responses to both the CS+ and CS− at the beginning of extinction, decreasing to become comparable to the other cluster groups by the end of the task (Figure 3H).

**Voxel-Wise Whole-Brain Comparison of Cluster Groups**

Finally, to identify brain regions outside the primary regions of interest included in the clustering, we conducted whole-brain analysis in the combined sample of 125 participants (Figure 4; see also Table S4 in the online supplement), comparing the three replicated cluster groups within the threat, reward, and inhibition fMRI tasks. The reactive/disinhibited cluster showed greater activation than the other two cluster groups in a mesopontine cluster overlapping with the median raphe nucleus and ventral tegmental area, as well as the hypothalamus, dACC, and insula in response to threat cues. In contrast, the low reward/high threat cluster showed greater activation in the left and right amygdala, hippocampus, and insula in response to threat cues. The reactive/disinhibited cluster also showed greater reactivity than the other two cluster groups in the amygdala, hippocampus, and rostral anterior cingulate cortex in response to reward. The inhibited cluster showed no region of greater activation compared with the other two cluster groups.

## DISCUSSION

In a well-characterized cohort followed longitudinally in the aftermath of trauma, we identified participant clusters in a manner that was agnostic to standard diagnostic categories for posttrauma outcomes using fMRI across several neurocognitive dimensions of interest, including threat, reward, and inhibition. In the discovery cohort of motor vehicle accident survivors, four clusters were

[a] The clusters showed differences in a multivariate profile of outcomes from 2 weeks to 6 months posttrauma (F=2.26, df=3, 1206, p=0.008). Panel A shows mental health profiles for each cluster, revealing standardized values for each outcome rescaled to a 0–1 scale. Because there was no interaction with time point, cluster profiles are collapsed across the 2-week, 8-week, 3-month, and 6-month study visits. Panel B shows how the clusters differed in the longitudinal model of posttraumatic stress disorder (PTSD) symptom severity, with the highest symptoms in the reactive/disinhibited cluster. The mean PTSD Checklist total score for each cluster over the assessment time points is shown, and gray shading shows 95% confidence intervals. The clusters showed no differences for univariate longitudinal models of depression symptoms (panel C), dissociative symptoms (panel D), or impulsivity (panel F). Panel E shows how the clusters differed in the longitudinal model of anxiety symptom severity, with highest symptoms among individuals in the inhibited cluster. Panel G shows the fear-potentiated startle response during the fear-conditioning paradigm conducted 2 weeks posttrauma. Fear conditioning to the conditioned stimulus (CS)+ danger cue and the CS− safety cue are shown over the course of three experimental blocks, with an overlay showing the main effect of CS type. The low reward/high threat cluster group showed significantly elevated fear-potentiated startle in response to both CS+ and CS− at the beginning of the task compared with the other clusters. Panel H shows the fear extinction task results, revealing fear-potentiated startle to the CS+ over the early and late trials of the task, with the overlay illustrating the main effect of block. Responses to the CS+ showed a significant decrease over time, consistent with extinction, but there were no differences between the four clusters. mo.=months; NA=noise alone.

**FIGURE 4. Whole-brain comparisons of the four cluster groups during the threat, reward, and inhibition tasks among trauma survivors in the Advancing Understanding of Recovery After Trauma study[a]**

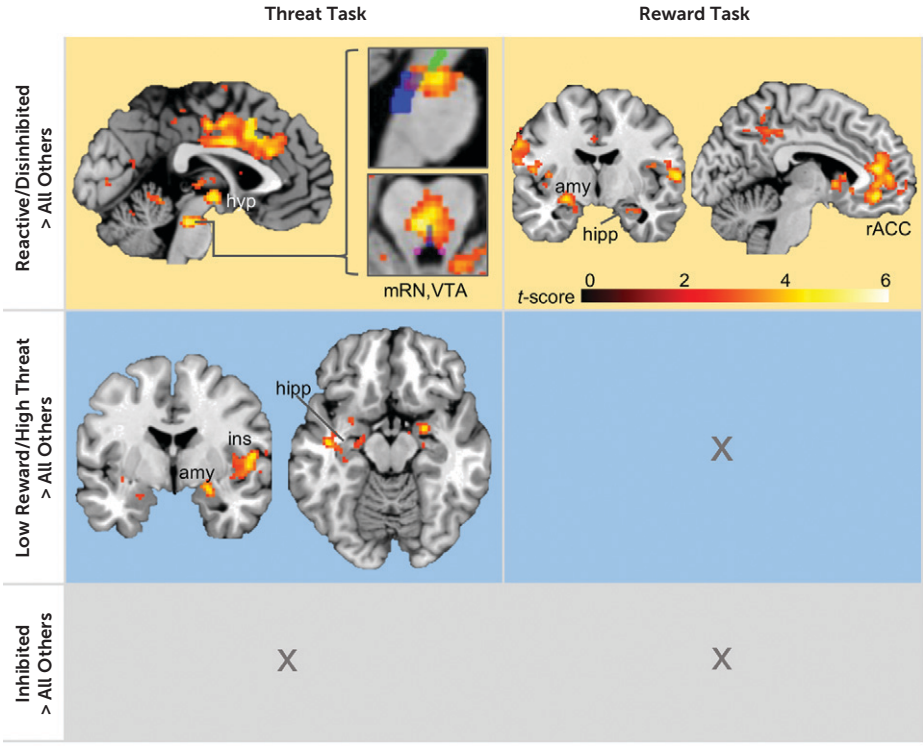


[a] Brain slices show the results of analysis of variance (ANOVA) comparing each cluster group with the other three groups (conducted separately for each task). ANOVAs revealed patterns of activation that were specific to each cluster group, outside of the regions of interest that were used in the clustering analysis. The reactive/disinhibited cluster showed significantly greater activation in the pontine reticular formation, which revealed overlap with the median raphe nucleus (mRN) (blue) and ventral tegmental area (VTA) (green) but not the locus ceruleus (violet) (45), as well as in the hypothalamus, during the threat task. The reactive/disinhibited cluster also showed greater rostral anterior cingulate cortex (rACC) activation than the other groups during the reward task. In contrast, the low reward/high threat cluster showed greater activation in the amygdala (amy), hippocampus (hipp), and insula (ins) in response to threat compared with the other groups. The high reward cluster showed greater activation in the amygdala, hippocampus, thalamus, and medial prefrontal regions during the reward task compared with the other groups. The inhibited cluster did not show any regions of greater activation compared with the other three groups on any of the individual functional MRI tasks. Brain slices show regions with greater activation in each cluster compared with the other three clusters (family-wise error corrected $p<0.05$). The gray "X" indicates that there was no significant difference in activation between the group of interest and the other three groups. For the inhibition task, there were no group-related differences. A full listing of all significant clusters and associated statistics is presented in Table S4 in the online supplement.

observed, and three were replicated in a cohort with a wider variety of index traumas. Given the timing at 2 weeks posttrauma, the clustering likely reflects a combination of traits that predate the trauma, as well as acute stress responses in the wake of the traumatic event. The clusters were not related to the demographic characteristics and background variables of the participants (e.g., gender, childhood trauma) but could still plausibly reflect pretrauma factors, such as genetics, family history, or temperament (40). Our findings confirmed the hypothesis that clusters may be associated with different posttrauma outcomes: different longitudinal patterns emerged over the first 6 months posttrauma, with the reactive/disinhibited cluster associated with subsequent heightened symptoms of PTSD/hypervigilance and anxiety. In addition, these findings represent an important step toward defining a neuroimaging-based longitudinal prediction model for stress-related resilience and vulnerability.

Our results suggest that an unsupervised forward-inference model is tractable for modeling heterogeneity in stress-related psychiatric outcomes, despite the lack of constraints on the model. We used very simple and transparent tools for clustering, uninformed by psychiatric symptoms or diagnoses, and found strong evidence for overlap (65%) in the cluster solutions arising from two fully independent hierarchical clustering solutions in different subcohorts. This level of overlap is consistent with cluster replication levels seen in larger brain-based clustering efforts, such as in the Adolescent Brain Cognitive Development study (41), and suggests that multivariate task-based fMRI data contain consistent information about individual differences. In fact, a major value of this study is its demonstration of task-based fMRI as a useful tool for mapping psychiatric heterogeneity. Task-based fMRI may not be needed to identify unitary biomarkers, such as for a diagnosis (e.g., PTSD) or a symptom (e.g., hyperarousal), where resting-state MRI is

likely preferable for its rich information on neural circuit function and low barriers to translation. However, for the purposes of resolving heterogeneity, task fMRI shows clear strengths. For example, the signal from the amygdala was clearly uncorrelated in threat tasks compared with reward tasks (Figure 2A,B), and this variability was important in resolving the clusters. Such information would not have been apparent from analyses of intrinsic network activity.

### Interpretation of the Biotypes

The reactive/disinhibited cluster was the most interesting candidate as a risk-related biotype. Individuals in this cluster showed threat hyperreactivity, particularly in the insula and dACC, accompanied by high NAcc reward reactivity, as well as higher subsequent PTSD symptoms. This was partly contrary to previous findings showing that lower NAcc reward response predicted subsequent PTSD (16). Threat and reward reactivity have rarely been assessed concurrently in previous studies of trauma and related outcomes. However, preclinical findings indicate that interacting pathways regulate both threat and reward reactivity. For example, stress-related hyperactivity of the basolateral amygdala can directly influence NAcc function via direct efferent projections (42) and change reward-seeking behaviors (43). Participants in the reactive/disinhibited cluster also showed greater activation in the reticular nuclei (median raphe, ventral tegmental area) during the threat task. The reticular formation stimulates wakefulness and arousal (44, 45). The role of these nuclei in dopamine and serotonin synthesis may point toward tailored intervention opportunities for the future; early studies are exploring dopaminergic modulation to treat PTSD (46).

The fMRI features observed in the low reward/high threat cluster included moderate responsivity to threat dominated by sgACC activation, along with markedly low reactivity to reward. Reduced reward responsivity in the NAcc, amygdala, and OFC is characteristic of major depressive disorder (47), as is sgACC hyperreactivity to sadness-inducing stimuli. The heightened fear-potentiated startle shown by this group during early fear acquisition and extinction is consistent with patterns previously observed in comorbid PTSD and major depressive disorder (27), which is more common posttrauma than each disorder alone (48). This cluster group also showed greater threat reactivity in the amygdala, insula, and hippocampus in whole-brain analyses compared with the other cluster groups. Together, the findings suggest the possibility that PTSD-related symptom groups may be divided into a low reward/high threat group driven more by cortical function, and a reactive/disinhibited group, driven more by brainstem nuclei.

Participants in the inhibited cluster appeared to be most consistent with active coping, with low threat reactivity accompanied by relatively high vmPFC and hippocampus engagement during inhibition. Individual features of this pattern have previously been associated with resilience. For example, lower amygdala threat reactivity predicts lower future PTSD symptoms (12, 13). Similarly, greater vmPFC and hippocampal activation during inhibition has been associated with resilience (22, 26). Our findings indicate that some individuals show the combined profile in the acute posttrauma period. However, this was the smallest cluster, and it is possible that inhibition as an adaptation to the stress of the index trauma had not yet fully emerged by 2 weeks posttrauma. As data collection continues, the AURORA study will include additional neuroimaging 6 months posttrauma, allowing a window into the further development of these profiles.

Participants in the high reward cluster showed high reward reactivity, low threat reactivity, and low inhibition, a pattern suggesting preserved positive affect in the context of low top-down regulation. However, this pattern may only be observed when the emotional impact of trauma is relatively low, and this cluster was not observed in the replication cohort.

### Limitations

To reduce participant burden, symptom assessments were abbreviated and based on self-report. This limited our ability to directly compare the outcomes to gold-standard assessments of psychiatric disorders. However, future work could apply these biotypes to archival data with interview-based assessments to extend our findings. Additionally, with sample sizes of 69 participants in the discovery cohort and 77 in the replication cohort, the study may be underpowered. However, we are encouraged that three clusters were replicated, indicating generalizability even across different types of trauma.

## CONCLUSIONS

Neuroimaging phenotypes emerging in the early aftermath of trauma are associated with risk of or resilience to trauma-related psychopathology. Contrary to our initial predictions that heightened threat and blunted reward reactivity may reflect stress vulnerability, a cluster showing heightened reactivity to both threat and reward was associated with the subsequent maintenance of the highest levels of PTSD symptoms. Heightened reward reactivity in the early aftermath of a major stressor may be an underexplored risk mechanism for the development of stress-related disorders. The biotypes identified here, with further development to assess normative values and precision, may provide important information about targeted interventions to address different forms of future stress-related psychopathology.

### AUTHOR AND ARTICLE INFORMATION

Department of Psychiatry and Behavioral Sciences, Emory University, Atlanta (Stevens, van Rooij, Ely, Roeckner, Vincent); Division of Depression and Anxiety, McLean Hospital, Belmont, Mass. (Harnett, Lebois, Ressler); Department of Psychiatry, Harvard Medical School, Boston (Harnett, Lebois, Pizzagalli, Ressler); Departments of Emergency Medicine and Health Services, Policy, and Practice, Alpert Medical School of Brown University, Rhode Island Hospital, and the Miriam Hospital, Providence, R.I. (Beaudoin); Department of Anesthesiology, Institute of Trauma Recovery, University of North Carolina, Chapel Hill (An,

Linnstaedt, McLean); Department of Biostatistics, Gillings School of Global Public Health, University of North Carolina, Chapel Hill (Zeng); Departments of Psychiatry and Neurology, University of California, San Francisco (Neylan); Department of Biomedical Informatics, Emory University School of Medicine, Atlanta (Clifford); Institute for Technology in Psychiatry (Germine) and Department of Psychiatry (Rauch), McLean Hospital, Belmont, Mass.; Department of Emergency Medicine, Henry Ford Health System, Detroit (Lewandowski); Department of Emergency Medicine, Vanderbilt University Medical Center, Nashville, Tenn. (Storrow); Department of Emergency Medicine, University of Florida College of Medicine, Jacksonville (Hendry, Sheikh); Department of Emergency Medicine, Indiana University School of Medicine, Indianapolis (Musey); Department of Emergency Medicine, University of Massachusetts Medical School, Worcester (Haran); Department of Emergency Medicine, Cooper Medical School of Rowan University, Camden, N.J. (Jones); Department of Emergency Medicine, College of Medicine and College of Nursing, University of Cincinnati, Cincinnati (Punches); Department of Emergency Medicine and Center for Addiction Research, University of Cincinnati College of Medicine, Cincinnati (Lyons); Departments of Emergency Medicine and Surgery, Division of Acute Care Surgery, University of Alabama School of Medicine, Birmingham (Kurz); Center for Injury Science, University of Alabama, Birmingham (Kurz); Department of Emergency Medicine, Boston Medical Center, Boston (McGrath); Departments of Surgery (Pascual) and Neurosurgery (Pascual), Perelman School of Medicine, University of Pennsylvania, Philadelphia; Department of Emergency Medicine, Einstein Health Care Network, Philadelphia (Datner); Department of Emergency Medicine, Jefferson University Hospitals, Philadelphia (Chang); Department of Emergency Medicine, Wayne State University, Detroit (Pearson); Department of Emergency Medicine, Massachusetts General Hospital, Boston (Peak); Department of Emergency Medicine, Saint Joseph Mercy Hospital, Ann Arbor, Mich. (Domeier); Department of Emergency Medicine, Wayne State University School of Medicine, Detroit (O'Neil); Department of Emergency Medicine, University of Massachusetts Medical School–Baystate, Springfield (Rathley); Department of Emergency Medicine, Beth Israel Deaconess Medical Center, Boston (Sanchez); Department of Emergency Medicine, Harvard Medical School, Boston (Sanchez); Department of Psychiatry, Yale School of Medicine, and U.S. Department of Veterans Affairs National Center for Posttraumatic Stress Disorder, Veterans Affairs Connecticut Healthcare System, New Haven, Conn. (Pietrzak); Department of Psychology, Yale University, New Haven, Conn. (Joorman); Department of Psychological and Brain Sciences, Washington University, St. Louis (Barch); Department of Biosciences and Neuroscience and Institute for Behavioral Medicine Research, Ohio State University Wexner Medical Center, Columbus (Sheridan); Department of Psychiatry, University of Pittsburgh, Pittsburgh (Luna); Departments of Anesthesiology and Internal Medicine–Rheumatology, University of Michigan Medical School, Ann Arbor (Harte); the Kolling Institute of Medical Research, Northern Clinical School, University of Sydney, and Faculty of Medicine and Health, University of Sydney, Sydney, Australia (Elliott); Physical Therapy and Human Movement Sciences, Feinberg School of Medicine, Northwestern University, Chicago (Elliott); Department of Psychology, Temple University, Philadelphia (Murty); Department of Psychiatry and Behavioral Neurosciences, Wayne State University, Detroit (Jovanovich); Department of Psychological Sciences, University of Missouri, St. Louis (Bruce); Department of Emergency Medicine, Washington University School of Medicine, St. Louis (House); Department of Health Care Policy, Harvard Medical School, Boston (Kessler); Department of Epidemiology, Harvard T.H. Chan School of Public Health, Boston (Koenen); Department of Emergency Medicine, University of North Carolina, Chapel Hill (McLean).

Send correspondence to Dr. Stevens (jennifer.stevens@emory.edu).

Dr. Jones has received funding from AstraZeneca, Hologic, Janssen, and Roche Diagnostics. Dr. Peak has received consulting fees from Akili Interactive Laboratories, BlackThorn Therapeutics, Boehringer Ingelheim, Posit Science, and Takeda Pharmaceuticals, and he has received an honorarium from Alkermes. Dr. Kessler has received funding for epidemiological studies from Sanofi-Aventis, and he has served as a consultant for DataStat, Sage Pharmaceuticals, and Takeda. Dr. Ressler has received consulting fees or sponsored research support from Alkermes, BrainsWay, and Genomind, and he serves on scientific advisory boards for Janssen, Takeda, and Verily. The other authors report no financial relationships with commercial interests.

Presented in part at the annual meeting of the American College of Neuropsychopharmacology, December 8–11, 2019, Orlando, Fla.

Dr. Sheikh is supported by the Florida Medical Malpractice Joint Underwriter's Association's Dr. Alvin E. Smith Safety of Healthcare Services, the NIH/National Institute on Aging Jacksonville Aging Studies Center (grant R33AG05654), and the Florida Blue Foundation. Dr. Elliott is supported by NIH (grants R01HD079076 and R03HD094577), the Eunice Kennedy Shriver National Institute of Child Health and Human Development, and the National Center for Medical Rehabilitation Research.

Supported by the Mayday Fund, NIMH (grants U01 MH110925, K00 MH119603, and K01 MH118467), the One Mind Foundation, and the U.S. Army Medical Research and Material Command. Data and/or research tools used in the preparation of this study were obtained from the NIMH Data Archive. The NIMH Data Archive is a collaborative informatics system created by NIH to provide a national resource to support and accelerate research in mental health (data set identifier, 10.15154/1521266).

The authors thank the trauma survivors who participated in the AURORA study.

This article reflects the views of the authors and may not reflect the opinions or views of NIH or of the submitters of original data to the NIMH Data Archive.

Received October 23, 2020; revisions received March 9 and April 21, 2021; accepted May 27, 2021; published online October 14, 2021.

## REFERENCES

1. Monroe SM, Simons AD: Diathesis-stress theories in the context of life stress research: implications for the depressive disorders. Psychol Bull 1991; 110:406–425
2. Howes OD, McCutcheon R, Owen MJ, et al: The role of genes, stress, and dopamine in the development of schizophrenia. Biol Psychiatry 2017; 81:9–20
3. Talbot LS, Maguen S, Metzler TJ, et al: Cognitive behavioral therapy for insomnia in posttraumatic stress disorder: a randomized controlled trial. Sleep (Basel) 2014; 37:327–341
4. Papst L, Binder EB: Stress Resilience. Amsterdam, Elsevier, 2020, pp 197–207
5. Galatzer-Levy IR, Bryant RA: 636,120 ways to have posttraumatic stress disorder. Perspect Psychol Sci 2013; 8:651–662
6. Zoellner LA, Pruitt LD, Farach FJ, et al: Understanding heterogeneity in PTSD: fear, dysphoria, and distress. Depress Anxiety 2014; 31:97–106
7. Mclean SA, Ressler K, Koenen KC, et al: The AURORA Study: a longitudinal, multimodal library of brain biology and function after traumatic stress exposure. Mol Psychiatry 2020; 25:283–296
8. Drysdale AT, Grosenick L, Downar J, et al: Resting-state connectivity biomarkers define neurophysiological subtypes of depression. Nat Med 2017; 23:28–38
9. Sellnow K, Sartin-Tarm A, Ross MC, et al: Biotypes of functional brain engagement during emotion processing differentiate heterogeneity in internalizing symptoms and interpersonal violence histories among adolescent girls. J Psychiatr Res 2020; 121:197–206
10. Clementz BA, Sweeney JA, Hamm JP, et al: Identification of distinct psychosis biotypes using brain-based biomarkers. Am J Psychiatry 2016; 173:373–384

11. Dinga R, Schmaal L, Penninx BWJH, et al: Evaluating the evidence for biotypes of depression: methodological replication and extension of. Neuroimage Clin 2019; 22:101796
12. Stevens JS, et al: Amygdala reactivity and anterior cingulate habituation predict PTSD symptom maintenance after acute civilian trauma. Biol Psychiatry 2017; 81:1023–1029
13. Admon R, Lubin G, Stern O, et al: Human vulnerability to stress depends on amygdala's predisposition and hippocampal plasticity. Proc Natl Acad Sci USA 2009; 106:14120–14125
14. McLaughlin KA, Busso DS, Duys A, et al: Amygdala response to negative stimuli predicts PTSD symptom onset following a terrorist attack. Depress Anxiety 2014; 31:834–842
15. Raij TT, Mäntylä T, Mantere O, et al: Cortical salience network activation precedes the development of delusion severity. Psychol Med 2016; 46:2741–2748
16. Admon R, Lubin G, Rosenblatt JD, et al: Imbalanced neural responsivity to risk and reward indicates stress vulnerability in humans. Cereb Cortex 2013; 23:28–35
17. Stringaris A, Vidal-Ribas Belil P, Artiges E, et al: The brain's response to reward anticipation and depression in adolescence: dimensionality, specificity, and longitudinal predictions in a community-based sample. Am J Psychiatry 2015; 172:1215–1223
18. Hanson JL, Hariri AR, Williamson DE: Blunted ventral striatum development in adolescence reflects emotional neglect and predicts depressive symptoms. Biol Psychiatry 2015; 78:598–605
19. Gaffrey MS, Barch DM, Bogdan R, et al: Amygdala reward reactivity mediates the association between preschool stress response and depression severity. Biol Psychiatry 2018; 83:128–136
20. Brassen S, Kalisch R, Weber-Fahr W, et al: Ventromedial prefrontal cortex processing during emotional evaluation in late-life depression: a longitudinal functional magnetic resonance imaging study. Biol Psychiatry 2008; 64:349–355
21. Dickie EW, Brunet A, Akerib V, et al: Neural correlates of recovery from post-traumatic stress disorder: a longitudinal fMRI investigation of memory encoding. Neuropsychologia 2011; 49:1771–1778
22. van Rooij SJH, Stevens JS, Ely TD, et al: The role of the hippocampus in predicting future PTSD symptoms in recently traumatized civilians. Biol Psychiatry 2018; 84:106–115
23. Gilam G, Lin T, Fruchter E, et al: Neural indicators of interpersonal anger as cause and consequence of combat training stress symptoms. Psychol Med 2017; 47:1561–1572
24. van Rooij SJH, Ravi M, Ely TD, et al: Hippocampal activation during contextual fear inhibition related to resilience in the early aftermath of trauma. Behav Brain Res 2021; 408:113282
25. Speer ME, Bhanji JP, Delgado MR: Savoring the past: positive memories evoke value representations in the striatum. Neuron 2014; 84:847–856
26. Jovanovic T, Ely T, Fani N, et al: Reduced neural activation during an inhibition task is associated with impaired fear inhibition in a traumatized civilian sample. Cortex 2013; 49:1884–1891
27. Jovanovic T, Norrholm SD, Blanding NQ, et al: Impaired fear inhibition is a biomarker of PTSD but not depression. Depress Anxiety 2010; 27:244–251
28. Milad MR, Pitman RK, Ellis CB, et al: Neurobiological basis of failure to recall extinction memory in posttraumatic stress disorder. Biol Psychiatry 2009; 66:1075–1082
29. Esteban O, Markiewicz CJ, Blair RW, et al: fMRIPrep: a robust preprocessing pipeline for functional MRI. Nat Methods 2019; 16:111–116
30. Pruim RHR, Mennes M, Buitelaar JK, et al: Evaluation of ICA-AROMA and alternative strategies for motion artifact removal in resting state fMRI. Neuroimage 2015; 112:278–287
31. Rousseeuw PJ: Silhouettes: a graphical aid to the interpretation and validation of cluster analysis. J Comput Appl Math 1987; 20:53–65
32. Hartigan JA: Clustering Algorithms. Hoboken, NJ, John Wiley and Sons, 1975
33. Hennig C: Cluster-wise assessment of cluster stability. Comput Stat Data Anal 2007; 52:258–271
34. Ripley BD: Pattern Recognition and Neural Networks. Cambridge, UK, Cambridge University Press, 2007
35. Kuhn M: Building predictive models in R using the caret package. J Stat Softw 2008; 28:1–26
36. Joormann J, McLean SA, Beaudoin FL, et al: Socio-demographic and trauma-related predictors of depression within eight weeks of motor vehicle collision in the AURORA study. Psychol Med (Online ahead of print, October 29, 2020)
37. Kessler RC, Ressler KJ, House SL, et al: Socio-demographic and trauma-related predictors of PTSD within 8 weeks of a motor vehicle collision in the AURORA study. Mol Psychiatry (Online ahead of print, October 19, 2020)
38. Orben A, Lakens D: Crud (re)defined. Adv Methods Pract Psychol Sci 2020; 3:238–247
39. Norrholm SD, Jovanovic T, Olin IW, et al: Fear extinction in traumatized civilians with posttraumatic stress disorder: relation to symptom severity. Biol Psychiatry 2011; 69:556–563
40. Ioannidis K, Askelund AD, Kievit RA, et al: The complex neurobiology of resilient functioning after childhood maltreatment. BMC Med 2020; 18:32
41. Hong S-J, Sisk LM, Caballero C, et al: Decomposing complex links between the childhood environment and brain structure in school-aged youth. Dev Cogn Neurosci 2021; 48:100919
42. McDonald AJ: Topographical organization of amygdaloid projections to the caudatoputamen, nucleus accumbens, and related striatal-like areas of the rat brain. Neuroscience 1991; 44:15–33
43. Sharp BM: Basolateral amygdala and stress-induced hyperexcitability affect motivated behaviors and addiction. Transl Psychiatry 2017; 7:e1194–e1194
44. Magoun HW: An ascending reticular activating system in the brain stem. AMA Arch Neurol Psychiatry 1952; 67:145–154, discussion 167–171
45. Edlow BL, Takahashi E, Wu O, et al: Neuroanatomic connectivity of the human ascending arousal system critical to consciousness and its disorders. J Neuropathol Exp Neurol 2012; 71:531–546
46. Cisler JM, Privratsky AA, Sartin-Tarm A, et al: L-DOPA and consolidation of fear extinction learning among women with posttraumatic stress disorder. Transl Psychiatry 2020; 10:287
47. Pizzagalli DA, Holmes AJ, Dillon DG, et al: Reduced caudate and nucleus accumbens response to rewards in unmedicated individuals with major depressive disorder. Am J Psychiatry 2009; 166:702–710
48. Caramanica K, Brackbill RM, Liao T, et al: Comorbidity of 9/11-related PTSD and depression in the World Trade Center Health Registry 10–11 years postdisaster. J Trauma Stress 2014; 27:680–688

**Supplementary Material to "Brain-based biotypes of psychiatric vulnerability in the acute aftermath of trauma"**

## 1. Supplementary Methods

1.1 Psychometric assessment

Trauma severity was measured using an Injury Severity Score (ISS) which takes into account multiple injuries and anatomical regions based on the Abbreviated Injury Scale(Gennarelli & Wodzin, 2006). The AIS codes single injuries based by anatomic location and relative severity. Participants also rated their chance of dying during the index trauma on a scale of 0-10 (0 - "life was not threatened at all"; 10 - "came very close to being killed or easily could have been killed"). Participants were classified as experiencing head trauma if the individual reported hitting head, and being dazed, confused, or in a fog, or having amnesia for some of the event, or loss of consciousness (all individual self-report questions administered in the ED), following criteria for minor traumatic brain injury diagnosis according to the American Congress of Rehabilitation Medicine. General physical health status of the participant was assessed for the 30 days pre-trauma, with a derived normative score based on questions from the 12-Item Short Form Health Survey (SF-12)(Ware Jr, Kosinski, & Keller, 1996). The Childhood Trauma Questionnaire (CTQ) was administered 2 weeks post-trauma(Bernstein & Fink, 1998). This self-report measure assesses 5 types of childhood maltreatment: emotional abuse, physical abuse, sexual abuse, emotional neglect, and physical neglect. The AURORA study used an abbreviated version with 11 of the 28 items in the CTQ: 2 items each from the physical neglect, emotional neglect, emotional abuse, and physical abuse subtype and 3 items from the sexual abuse subtype. Items were summed to create a CTQ total score.

PTSD symptoms were assessed using the PTSD Symptom Checklist for DSM-5 (PCL-5)(Weathers et al., 2013). The PCL-5 is a 20 item self-report questionnaire assessing the presence and severity of hyperarousal, intrusions, negative cognitions, and avoidance symptoms. Each item was rated from 0 (not at all) to 4 (extremely), and items were summed to create a 0-80 scale. Depression symptoms were assessed using the Patient-Reported Outcomes Measurement Information System (PROMIS) Depression instrument (Pilkonis et al., 2011) with eight items evaluating depressive symptom frequency scored from 1 (never) to 5 (always). Items were summed and converted to a T-score. Dissociation was assessed using the Brief Dissociative Experiences Scale – Modified (DES-B)(Carlson & Putnam, 1993). The 8-item DES-B was abbreviated to include 2 items reflecting common forms of dissociation. Participants reported how often they had the following experiences: People, objects, or the world around you seemed strange or unreal, and You felt as though you were looking through a fog so that people and things seemed far away or unclear, on a scale of 1 (none of the time) - 5 (all or almost all of the time). The 2 items were summed to create a total dissociative experiences score. Impulsivity was assessed using the Impulsive Behavior Scale – Short Form (SUPPS-P; Cyders, Littlefield, Coffey & Karyadi, 2014). The 20-item scale was abbreviated to assess 8 items, measuring negative urgency, lack of perseverance items, lack of premeditation, and positive urgency, on a scale of 0 (never) to 4 (very often). A total SUPPS-P score was calculated by summing the items. Anxiety symptoms were assessed using 4 items from the PROMIS Anxiety bank (Pilonkis et al., 2011), assessing anxious feelings, worry, difficulty relaxing, and feeling tense, on a scale of 0 (none of the time) to 5 (all or almost all of the time).

Surveys were sent to participants via text or email for self-completion, or were completed with the assistance of telephone interviewers based on participant preference. All scales queried symptoms occurring in the past 2 weeks (2-week survey) or past 30 days (ED, 8-week, 3-month, and 6-month surveys). Missing values were imputed using multiple imputation in Hmisc v4.3, with 5 iterations of a 3-knot model, and missing values were replaced with values from the final iteration. N=7 participants missing data at all 4 timepoints were omitted from the analysis of mental health outcome trajectories; this appeared independent of subsequent biotyping assignments with n=2 each from clusters 1/2/4, and n=1 from cluster 3.

1.2 fMRI data processing and analyses

1.2.1 MRI data conversion and quality control. DICOM images were converted to NIFTI format with Brain Imaging Data Structure (BIDS) nomenclature using dcm2niix (Li et al. 2016) and were visually inspected for conversion errors and data exclusion criteria (e.g., signal drop-out from Falx calcification, anatomical abnormalities). Further quality control was achieved by running the MRIQC pipeline (version 0.10.4 in a Docker container) (Esteban et al. 2017a) on the structural and functional images.
Results included in this manuscript come from preprocessing performed using fMRIPrep 1.2.2 (Esteban, Blair, et al. (2017); Esteban, Markiewicz, et al. (2018); RRID:SCR_016216), which is based on Nipype 1.1.5 (Gorgolewski et al. (2011); Gorgolewski et al. (2017); RRID:SCR_002502). In order to maintain consistency in preprocessing throughout the duration of data collection, FMRIPrep was run in a Docker container retaining the version that was newest at the initiation of the study.

1.2.2 Anatomical data preprocessing. The T1-weighted (T1w) images were corrected for intensity non-uniformity using N4BiasFieldCorrection (Tustison et al. 2010, ANTs 2.2.0), and used as T1w-reference throughout the workflow. The T1w-reference was then skull-stripped using antsBrainExtraction.sh (ANTs 2.2.0), and OASIS as target template. Brain surfaces were reconstructed using recon-all (FreeSurfer 6.0.1, RRID:SCR_001847, Dale, Fischl, and Sereno 1999), and the brain mask estimated previously was refined with a custom variation of the method to reconcile ANTs-derived and FreeSurfer-derived segmentations of the cortical gray-matter of Mindboggle (RRID:SCR_002438, Klein et al. 2017). Spatial normalization to the ICBM 152 Nonlinear Asymmetrical template version 2009c (Fonov et al. 2009, RRID:SCR_008796) was performed through nonlinear registration with antsRegistration (ANTs 2.2.0, RRID:SCR_004757, Avants et al. 2008), using brain-extracted versions of both T1w volume and template. Brain tissue segmentation of cerebrospinal fluid (CSF), white-matter (WM) and gray-matter (GM) was performed on the brain-extracted T1w using fast (FSL 5.0.9, RRID:SCR_002823, Zhang, Brady, and Smith 2001).

1.2.3 Functional data preprocessing. For each of the 4 BOLD runs found per subject (across all tasks and sessions), the following preprocessing was performed. First, a reference volume and its skull-stripped version were generated using a custom methodology of fMRIPrep. The BOLD reference was then co-registered to the T1w reference using bbregister (FreeSurfer) which implements boundary-based registration (Greve and Fischl, 2009). Co-registration was configured with nine degrees of freedom to account for distortions remaining in the BOLD reference. Head-motion parameters with respect to the BOLD reference (transformation matrices, and six corresponding rotation and translation parameters) are estimated before any spatiotemporal filtering using mcflirt (FSL 5.0.9, Jenkinson et al. 2002). BOLD runs were slice-time corrected using 3dTshift from AFNI 20160207 (Cox, 1996, RRID:SCR_005927). The BOLD time-series (including slice-timing correction) were resampled onto their original, native space by applying a single, composite transform to correct for head-motion and susceptibility distortions. These resampled BOLD time-series will be referred to as ‘preprocessed BOLD in original space’, or just ‘preprocessed BOLD.’ First, a reference volume and its skull-stripped version were generated using a custom methodology of fMRIPrep. Automatic removal of motion artifacts using independent component analysis (ICA-AROMA, Pruim et al. 2015) was performed on the preprocessed BOLD on MNI space time-series after removal of non-steady state volumes and spatial smoothing with an isotropic, Gaussian kernel of 6mm FWHM (full-width half-maximum). To deal with cases in which motion was likely too high for effective ICA-based correction, we also implemented an overall motion threshold was set such that data from a particular task (Threat, Inhibition, Reward, Resting State) were excluded from analysis entirely for any participant with more than 15% of volumes exceeding 1mm FD.

Although not used in our current analyses, these regressors and corresponding non-denoised and unsmoothed images are available for alternative analyses in the future. These noise regressors were generated as follows:The BOLD time-series were resampled to MNI152NLin2009cAsym standard space, generating a preprocessed BOLD run in MNI152NLin2009cAsym space. First, a reference volume and its skull-stripped version were generated using a custom methodology of fMRIPrep. Several confounding time-series were calculated based on the preprocessed BOLD: framewise displacement (FD), DVARS and three region-wise global signals. FD and

DVARS are calculated for each functional run, both using their implementations in Nipype (following the definitions by Power et al. 2013). The three global signals are extracted within the CSF, the WM, and the whole-brain masks.

Additionally, a set of physiological regressors were extracted to allow for component-based noise correction (CompCor, Behzadi et al. 2007). Principal components are estimated after high-pass filtering the preprocessed BOLD time-series (using a discrete cosine filter with a 128s cut-off) for the two CompCor variants: temporal (tCompCor) and anatomical (aCompCor). Six tCompCor components are then calculated from the top 5% variable voxels within a mask covering the subcortical regions. This subcortical mask is obtained by heavily eroding the brain mask, which ensures it does not include cortical GM regions. For aCompCor, six components are calculated within the intersection of the aforementioned mask and the union of CSF and WM masks calculated in T1w space, after their projection to the native space of each functional run (using the inverse BOLD-to-T1w transformation). The head-motion estimates calculated in the correction step were also placed within the corresponding confounds file. The BOLD time-series, were resampled to surfaces on the following spaces: fsaverage5. All resamplings can be performed with a single interpolation step by composing all the pertinent transformations (i.e. head-motion transform matrices, susceptibility distortion correction when available, and co-registrations to anatomical and template spaces). Gridded (volumetric) resampling was performed using antsApplyTransforms (ANTs), configured with Lanczos interpolation to minimize the smoothing effects of other kernels (Lanczos 1964). Non-gridded (surface) resampling was performed using `mri_vol2surf`(FreeSurfer). Many internal operations of fMRIPrep use Nilearn 0.4.2 (Abraham et al. 2014, RRID:SCR_001362), mostly within the functional processing workflow.

1.2.4 First level models. Initial statistical modeling was conducted in SPM12. For the Threat task, blocks of fearful and neutral stimuli were modeled with separate boxcar functions representing the onset and 8000 ms duration of each block, convolved with a canonical hemodynamic response function. Contrasts of fearful>neutral face blocks were used for ROI extraction. For the Inhibition task, correct Go and correct No-Go trials were each modeled in an event-related design (0ms event duration), and incorrect Go and No-Go trials were modeled separately. Contrasts of correct No-Go > correct Go trials were used for ROI extraction. For the Reward task, gain and loss trials were modeled as separate experimental conditions in an event-related design, and any trial on which the participant neglected to make a button press was modeled in an error condition. Contrasts of Gain > Loss were used for ROI extraction. In all first-level models, white matter, CSF and global signal time courses were included as nuisance regressors, as this has been shown to provide a good balance of noise correction from motion/physiological sources while retaining signal quality, after ICA-AROMA (Satterthwaite et al., 2019).

1.2.5 Data extraction from regions of interest (ROIs). The mean across all voxels in each ROI was extracted from first-level contrasts using rex (https://www.nitrc.org/projects/rex/). ROIs were defined bilaterally, using anatomical boundaries. For Threat, ROIs included the amygdala(Tyszka & Pauli, 2016), insula(Tzourio-Mazoyer et al., 2002), and sgACC and dACC defined as Brodmann Areas 25 and 32 respectively, based on translational work showing that these are the primate cortical areas corresponding to regions that inhibit (BA 25) or express fear (BA 32)(Tang et al., 2019). For Reward, ROIs included the NAcc(Pauli, Nili, & Tyszka, 2018), OFC(Fischl et al., 2004), and amygdala(Tyszka & Pauli, 2016). For Inhibition, ROIs included the hippocampus(Hammers et al., 2003), and a 6mm sphere in vmPFC (centered at x=-4,y=44,z=-4) based on prior work with this task defining an area whose activation in the No-Go>Go contrast is correlated with inhibition of fear to unreinforced vs reinforced cues(Jovanovic et al., 2013). We did not require that all ROIs show significant task-related activation, as some regions with high inter-individual variability may not be significantly activated in group-level analyses.

Prior to clustering, fMRI data from each ROI were z-scored to minimize range effects. Outliers were replaced with a cap score at M±3SD. Scaling and outlier correction were conducted separately for discovery and replication cohorts. For the purpose of visualizing the cluster solutions, a principal components analysis (PCA) was conducted using factoextra 1.0.5. For the PCA, ROI data from both discovery and replication samples was

combined to allow the cluster solutions for discovery and replication to be displayed in the same latent variable space. Examination of the loadings (**Table S1**) indicated that the first three PCs corresponded to threat (23% of the variance), reward (21%), and inhibition (12%).

1.2.6 Whole-brain analyses. Whole brain analyses were conducted to identify task-related activation for the threat, reward, and inhibition tasks. Analyses were corrected for multiple comparisons using an initial voxel-wise threshold of $p<0.005$, in combination with an extent threshold for clusters to allow a family-wise error rate of less than 5% ($p_{FWE}<0.05$). The cluster extent thresholds required for this level of correction were k=114 for threat, k=82 for reward, and k=116 for inhibition. In addition, after having identified cluster solutions using the limited input data from the ROIs, we then conducted whole-brain ANOVAs to identify additional differences between cluster groups outside of the a priori ROIs (1 model per task). To meet a FWE-corrected $p<.05$, the initial cluster-forming threshold was again set to $p<.005$ and the extent thresholds were k=164 for threat, k=146 for reward, and no clusters meeting FWE-correction for the inhibition task.

1.3 Fear-potentiated startle

Fear-potentiated startle data were included to provide more insight into the individual differences seen in each of the clusters. Individuals with chronic PTSD show noted differences from trauma-exposed control participants during fear learning as well as extinction, including heightened fear to safety cues during fear acquisition, and slower extinction (Jovanovic et al., 2009). These features may be apparent in the early aftermath of trauma, potentially contributing to the prolonged maintenance of high levels of fear to trauma cues.

Psychophysiological data were collected at the same visit as the fMRI scan 2 weeks posttrauma, using a Pavlovian fear conditioning procedure (Glover et al., 2012; Jovanovic et al., 2009). The unconditioned stimulus (US) was a 140 psi airblast with a 250ms duration, delivered to the neck. Conditioned stimuli (CS) were colored shapes presented on a computer screen; the reinforced CS+ was paired with the US on 100% of the trials, and the non-reinforced CS- was never paired with the US. To assess the startle eyeblink response, a 108 dB white noise burst was presented during every CS trial, and during noise-alone (NA) trials for the assessment of baseline startle response. The startle probe was presented six seconds after CS onset, followed by the US 0.5 s later. Conditioning consisted of three blocks of four trials of each type (NA, CS+, CS-). After a 10-minute delay, extinction consisted of four blocks with four trials of each type (CS+, CS-, NA) wherein the US never occurred. The startle eyeblink response was measured using electromyography of the right orbicularis oculi muscle. Fear-potentiated startle was calculated by subtracting the startle magnitude to the noise probe alone from the startle magnitude to the CS in each block of the experiment.

The startle eyeblink response was measured using electromyography (EMG) of the right orbicularis oculi muscle using a Biopac MP150 (Biopac Systems, Inc., Aero Camino, CA). Two 5 mm Ag/AgCl pre-gelled disposable electrodes were placed 1 cm below the participant's pupil and 1 cm inferior to the lateral canthus. Impedances < 6 kOhm were accepted, and data was recorded at 1 kHz. Using MindWare software (MindWare Technologies, Inc.; Gahanna, OH), EMG signals were amplified by a gain of 2000 and visually inspected for artifact. Startle magnitude was defined as the maximal contraction 20 to 200 ms following the startle probe presentation. Fear-potentiated startle (FPS) was calculated by subtracting the startle magnitude to the noise probe alone from the startle magnitude to the CS in each block of the experiment, for both acquisition and extinction.

## 2. Supplemental Results

2.1 Demographic and pre-trauma characteristics of the four clusters

Because of the unconstrained clustering approach, key demographic features may differ across the clusters, potentially contributing to the cluster solution. There was no association between cluster assignment and age ($F_{2,121}$=0.45, p=.64), gender ($\chi^2$ =0.38, p=.83), race/ethnicity ($\chi^2$ =6.39, p=.38), educational attainment ($\chi^2$ =23.44, p=.38), employment ($\chi^2$ =5.95, p=.65), income ($\chi^2$ =7.15, p=.71), BMI ($F_{2,121}$=0.23, p=.80), overall physical health prior to the trauma ($F_{2,119}$=1.39, p=.25), marital status ($\chi^2$ =5.52, p=.70), or childhood trauma exposure ($F_{2,121}$=0.86, p=.43). There was also no association between cluster assignment and features of the index trauma such as trauma type ($\chi^2$ =14.36, p=.57), participants' assessment of chance of dying ($F_{2,121}$=2.19, p=.12), or injury severity ($F_{2,121}$=1.25, p=.29). There were no differences in head trauma across clusters, $\chi^2$ = 1.08, p=.58. There was no relationship with the site of the MRI data collection, $\chi^2$ =4.59, p=.60, nor aspects of data quality for any of the three fMRI scans (**ST2**). Finally, there were no cluster-wise differences in the proportion of participants taking medications, or psychiatric medications specifically (**ST5**). The clusters therefore appear to reflect covert neurocognitive features, rather than demographic, health-related, trauma-related, or site-specific factors.

**Table S1. Principal Components Analysis for dataset including Cohort 1 + 2 – factor loadings**

| Task | ROI | PC1 (0.23) [a] | PC2 (0.21) | PC3 (0.12) | PC4 (0.11) | PC5 (0.09) | PC6 (0.08) | PC7 (0.06) | PC8 (0.06) | PC9 (0.04) |
|---|---|---|---|---|---|---|---|---|---|---|
| Threat | Amygdala | 0.35 | 0.00 | 0.14 | 0.31 | -0.37 | 0.29 | 0.72 | -0.09 | 0.15 |
| | Insula | 0.54 | 0.15 | 0.17 | -0.29 | 0.35 | -0.19 | -0.02 | 0.15 | 0.62 |
| | dACC | 0.56 | 0.12 | 0.05 | -0.07 | 0.20 | -0.22 | 0.09 | 0.04 | -0.75 |
| | sgACC | 0.44 | -0.27 | 0.11 | 0.39 | -0.17 | 0.31 | -0.65 | -0.13 | 0.04 |
| Inhibition | Hippocampus | -0.25 | -0.04 | 0.67 | 0.49 | 0.49 | -0.09 | 0.08 | -0.01 | -0.03 |
| | vmPFC | -0.06 | -0.24 | 0.66 | -0.59 | -0.35 | 0.04 | -0.04 | -0.12 | -0.11 |
| Reward | Nacc | -0.03 | 0.46 | 0.20 | 0.24 | -0.53 | -0.40 | -0.18 | 0.46 | 0.02 |
| | Amygdala | -0.06 | 0.49 | 0.12 | -0.15 | 0.16 | 0.75 | -0.08 | 0.34 | -0.11 |
| | OFC | -0.01 | 0.61 | 0.06 | 0.00 | -0.05 | -0.05 | -0.11 | -0.78 | 0.04 |

[a] Component (% variance in the original data accounted for by that component)

**Table S2. Analysis of cluster associations with MRI data quality, by fMRI task**

| Task | FD | DVARS | TSNR |
|---|---|---|---|
| Threat | $F_{1,121}$=1.17, p=0.31 | $F_{1, 121}$=0.90, p=0.41 | $F_{1, 121}$=0.33, p=0.72 |
| Inhibition | $F_{1, 121}$=1.11, p=0.33 | $F_{1, 121}$=0.14, p=0.86 | $F_{1, 121}$=0.31, p=0.73 |
| Reward | $F_{1, 121}$=0.10, p=0.90 | $F_{1, 121}$=0.10, p=0.90 | $F_{1, 121}$=0.29, p=0.75 |

Abbreviations: FD- Framewise displacement, DVARS- Standard deviation in the global signal, TSNR- Temporal signal-to-noise ratio

**Table S3. Model fit (QICC[a]) for cluster-based versus dimensional fMRI predictors of post-trauma outcome**

| Outcome | β PC1/PC2/PC3 | Dimensional model, QIC | Cluster-based model, QIC |
|---|---|---|---|
| PTSD | 1.21/0.63/-3.58 | 127153.83 | 129606.88 |
| Depression | 0.20/0.70/-1.80 | 49842.45 | 50801.76 |
| Dissociation | 0.14/-0.25/-0.65* | 1574.94 | 1564.82 |
| Anxiety | 0.60/-0.10/-0.82 | 8911.06 | 9379.86 |
| Impulsivity | 1.21/0.63/-3.58, all n.s. | 8680.61 | 8665.33 |

[a] QICC- Corrected Quasi Likelihood under Independence Model Criterion. Smaller values indicate better model fit
* = p<0.05.

**Table S4. Whole-brain comparisons of the four groups**

| Task | Group comparison | Region | HEM | x | y | z | Z | Volume (mm3) |
|---|---|---|---|---|---|---|---|---|
| Threat (Fearful > Neutral Faces) | 1 > (2, 4) | Mid. Cingulate G. | L | -4 | -14 | 42 | 6.30 | 110916 |
| | | Mid. Cingulate G. | R | 10 | 24 | 36 | 5.86 | |
| | | Supp. Motor Area | R | 2 | 14 | 46 | 5.45 | |
| | | Fusiform G., Hypothalamus, Occipital, Insula | R | 22 | -34 | -16 | 5.86 | 563436 |
| | | Rolandic Oper. | R | 62 | -10 | 12 | 5.57 | |
| | | Sup. Temporal G. | L | -38 | -24 | 0 | 5.46 | |
| | | Ventral Tegmental Area | L | -2 | -26 | -22 | 5.24 | 5022 |
| | | Median Raphe Nucleus | R | 4 | -22 | -28 | 4.25 | |
| | | Mesopontine | L | -10 | -20 | -28 | 4.19 | |
| | | Cuneus | L | -14 | -78 | 30 | 4.47 | 6210 |
| | | Cuneus | L | -12 | -70 | 22 | 3.31 | |
| | | Cuneus | L | -6 | -82 | 36 | 3.23 | |
| | | Inf. Occipital G. | L | -50 | -68 | -12 | 4.39 | 6804 |
| | | Inf. Temporal G. | L | -54 | -58 | -6 | 3.88 | |
| | | Inf. Occipital G. | L | -44 | -76 | -4 | 3.75 | |
| | | Sup. Occipital G. | R | 22 | -64 | 48 | 4.28 | 8532 |
| | | Sup. Parietal G. | R | 32 | -64 | 52 | 3.70 | |
| | | Sup. Occipital G. | R | 26 | -60 | 40 | 3.52 | |
| | | Caudate | L | -8 | 10 | 16 | 4.13 | 8370 |
| | | Caudate | R | 4 | 8 | 8 | 4.06 | |
| | | Thalamus | L | -12 | -4 | 4 | 3.95 | |
| | | Sup. Frontal G. | L | -22 | 12 | 62 | 4.05 | 7263 |
| | | Sup. Frontal G. | L | -20 | 20 | 52 | 3.47 | |
| | | Supp. Motor Area | L | -6 | 6 | 60 | 3.44 | |
| | | Sup. Frontal G. | L | -16 | 58 | 30 | 4.02 | 4833 |
| | | Sup. Frontal G. | L | -4 | 62 | 28 | 3.77 | |
| | | Sup. Frontal G. | L | -30 | 54 | 26 | 3.51 | |
| | | | | | | | | |
| | 2 > (1, 4) | Parahippocampal G. | R | 22 | -16 | -22 | 4.55 | 5292 |
| | | Amygdala | R | 24 | -4 | -16 | 4.16 | |
| | | Parahippocampal G. | R | 16 | -6 | -20 | 3.29 | |
| | | Rolandic Oper. | R | 54 | -2 | 6 | 4.29 | 9153 |
| | | Insula | R | 44 | 0 | -6 | 3.67 | |
| | | Temporal Pole | R | 60 | 4 | 2 | 3.31 | |
| | | Mid. Temporal G. | L | -42 | -14 | -16 | 4.25 | 7047 |
| | | Hippocampus | L | -28 | -16 | -20 | 3.50 | |
| | | Parahippocampal G. | L | -18 | -12 | -24 | 3.40 | |
| | | Supramarginal G. | L | -58 | -38 | 28 | 3.68 | 4428 |

| | | | | | | | | |
|---|---|---|---|---|---|---|---|---|
| | | Sup. Temporal G. | L | -44 | -32 | 18 | 3.63 | |
| | | Insula | L | -32 | -20 | 12 | 3.30 | |
| | | | | | | | | |
| | 4 > (1, 2) | * No significant clusters | | | | | | |
| | | | | | | | | |
| Reward (Monetary Gain > Loss) | 1 > (2, 4) | Caudate | R | 8 | 8 | -6 | 5.07 | 12069 |
| | | Caudate | L | -18 | 24 | 0 | 4.03 | |
| | | Putamen | R | 20 | 4 | -8 | 4.01 | |
| | | Ant. Cingulate G. | L | -6 | 42 | 12 | 4.82 | 40284 |
| | | Orbitofrontal G. | L | -8 | 40 | -10 | 4.80 | |
| | | Ant. Cingulate G. | R | 14 | 40 | 16 | 4.64 | |
| | | Fusiform G. | L | -34 | -26 | -18 | 4.76 | 3942 |
| | | Fusiform G. | L | -34 | -40 | -22 | 4.63 | |
| | | Fusiform G. | L | -30 | -36 | -16 | 3.17 | |
| | | Sup. Temporal G. | R | 66 | -6 | 6 | 4.72 | 25326 |
| | | Insula | R | 48 | 14 | -10 | 4.68 | |
| | | Rolandic Oper. | R | 36 | -20 | 18 | 4.59 | |
| | | Heschl G. | L | -36 | -24 | 14 | 4.50 | 25083 |
| | | Postcentral G. | L | -66 | -4 | 26 | 4.25 | |
| | | Postcentral G. | L | -64 | -20 | 18 | 4.24 | |
| | | Precuneus | L | -12 | -52 | 46 | 4.41 | 10044 |
| | | Sup. Parietal G. | L | -20 | -60 | 54 | 4.34 | |
| | | Precuneus | L | -2 | -44 | 40 | 3.75 | |
| | | Angular G. | L | -50 | -60 | 24 | 4.20 | 8505 |
| | | Angular G. | L | -46 | -72 | 42 | 3.93 | |
| | | Angular G. | L | -52 | -70 | 36 | 3.58 | |
| | | Parahippocampal | R | 20 | -16 | -22 | 4.15 | 3942 |
| | | Parahippocampal | R | 12 | -22 | -26 | 3.47 | |
| | | Hippocampus | R | 32 | -10 | -20 | 3.26 | |
| | | Mid. Cingulate G. | -- | 0 | -2 | 36 | 3.98 | 4995 |
| | | Mid. Cingulate G. | R | 12 | -16 | 40 | 3.81 | |
| | | Mid. Cingulate G. | -- | 0 | -18 | 36 | 3.34 | |
| | | Precuneus | R | 12 | -44 | 60 | 3.54 | 4077 |
| | | Precuneus | R | 6 | -38 | 56 | 3.50 | |
| | | Paracentral lobule | R | 14 | -40 | 48 | 2.88 | |
| | | | | | | | | |
| | 2 > (1, 4) | * No significant clusters | | | | | | |
| | | | | | | | | |
| | 4 > (1, 3) | * No significant clusters | | | | | | |
| | | | | | | | | |
| Inhibition (No-Go > Go) | No differences | | | | | | | |

| | | | | | | |
|---|---|---|---|---|---|---|
| across groups | | | | | | |

**Table S5. MRI scan sequence parameters by site**

| | **SITE1 SIEMENS TIM 3T TRIO (12 CHANNEL HEAD COIL)** | **SITE2 SIEMENS TIM 3T TRIO (12 CHANNEL HEAD COIL)** | **SITE3 SIEMENS MAGNETOM 3T PRISMA (20 CHANNEL HEAD COIL)** | **SITE4 SIEMENS 3T VERIO (12 CHANNEL HEAD COIL)** |
|---|---|---|---|---|
| **MODALITY** | | | | |
| **T1-WEIGHTED** | **TR** = 2530ms, **TEs** = 1.74/3.6/5.46/7.32ms, **TI** = 1260ms, **flip angle** = 7, **FOV** = 256mm, **slices** = 176, **Voxel size** = 1mm x 1mm x 1mm | **TR** = 2530ms, **TEs** = 1.74/3.6/5.46/7.32ms, **TI** = 1260ms, **flip angle** = 7, **FOV** = 256mm, **slices** = 176, **Voxel size** = 1mm x 1mm x 1mm | **TR** = 2300ms, **TE** = 2.96ms, **TI** = 900ms, **flip angle** = 9, **FOV** = 256mm, **slices** = 176, **Voxel size** = 1.2mm x 1.0mm x 12mm | **TR** = 2530ms, **TEs** = 1.74/3.65/5.51/7.72ms, **TI** = 1260ms, **flip angle** = 7, **FOV** = 256mm, **slices** = 176, **Voxel size** = 1mm x 1mm x 1mm |
| **FUNCTIONAL MRI** | **TR** = 2360ms, **TE** = 30ms, **flip angle** = 70, **FOV** = 212mm, **slices** = 44, **Voxel size** = 3mm x 2.72mm x 2.72mm, 0.5 mm gap | **TR** = 2360ms, **TE** = 30ms, **flip angle** = 70, **FOV** = 212mm, **slices** = 44, **Voxel size** = 3mm x 3mm x 3mm, 0.5 mm gap | **TR** = 2360ms, **TE** = 29ms, **flip angle** = 70, **FOV** = 212mm, **slices** = 44, **Voxel size** = 3mm x 2.72mm x 2.72mm, 0.5 mm gap | **TR** = 2360ms, **TE** = 30ms, **flip angle** = 70, **FOV** = 212mm, **slices** = 42, **Voxel size** = 3mm x 2.72mm x 2.72mm, 0.5 mm gap |

**Table S6. Medications taken at any point post-trauma, by cluster (N)**

| Medication type | Cluster 1 | Cluster 2 | Cluster 3 | Cluster 4 | Total |
|---|---|---|---|---|---|
| Acetaminophen | 1 | 4 | 0 | 1 | 6 |
| ACE Inhibitors | 3 | 3 | 2 | 0 | 8 |
| Antibiotics | 1 | 2 | 1 | 2 | 6 |
| Anticholinergics | 1 | 7 | 0 | 2 | 10 |
| Benzodiazepines | 0 | 3 | 1 | 1 | 5 |
| Beta blockers | 0 | 2 | 0 | 0 | 2 |
| Contraceptives | 1 | 1 | 0 | 1 | 3 |
| Non-steroidal anti-inflammatory | 6 | 11 | 3 | 5 | 25 |
| Opioids | 2 | 2 | 0 | 4 | 8 |
| Serotonin and norepinephrine reuptake inhibitors | 1 | 1 | 1 | 1 | 4 |
| Serotonin reuptake inhibitors | 1 | 5 | 0 | 3 | 9 |
| **Any medication**<br>$\chi^2$ =0.62, p=0.89 with Cluster 3<br>$\chi^2$ =0.41, p=0.81 without Cluster 3 | **10** | **21** | **6** | **11** | **48** |
| **Any psychoactive medication**<br>$\chi^2$ =2.40, p=0.49 with Cluster 3<br>$\chi^2$ =1.72, p=0.42 without Cluster 3 | **4** | **9** | **2** | **7** | **22** |

**Figure S1 Cluster number metrics for fMRI data collected 2 weeks post-trauma, for the discovery sample (a-b) and replication sample (c-d).**
(**a,b**) Weighted sum of squares for within-cluster point distances across a range of cluster solutions. The optimal solution following Hartigan's distance index is denoted with dotted line. (**c,d**) Silhouette width for a range of cluster solutions after hierarchical clustering using Wilk's criterion. Width summarizes the distance of points within a cluster relative to points outside the cluster. Dotted line indicates maximum silhouette width.

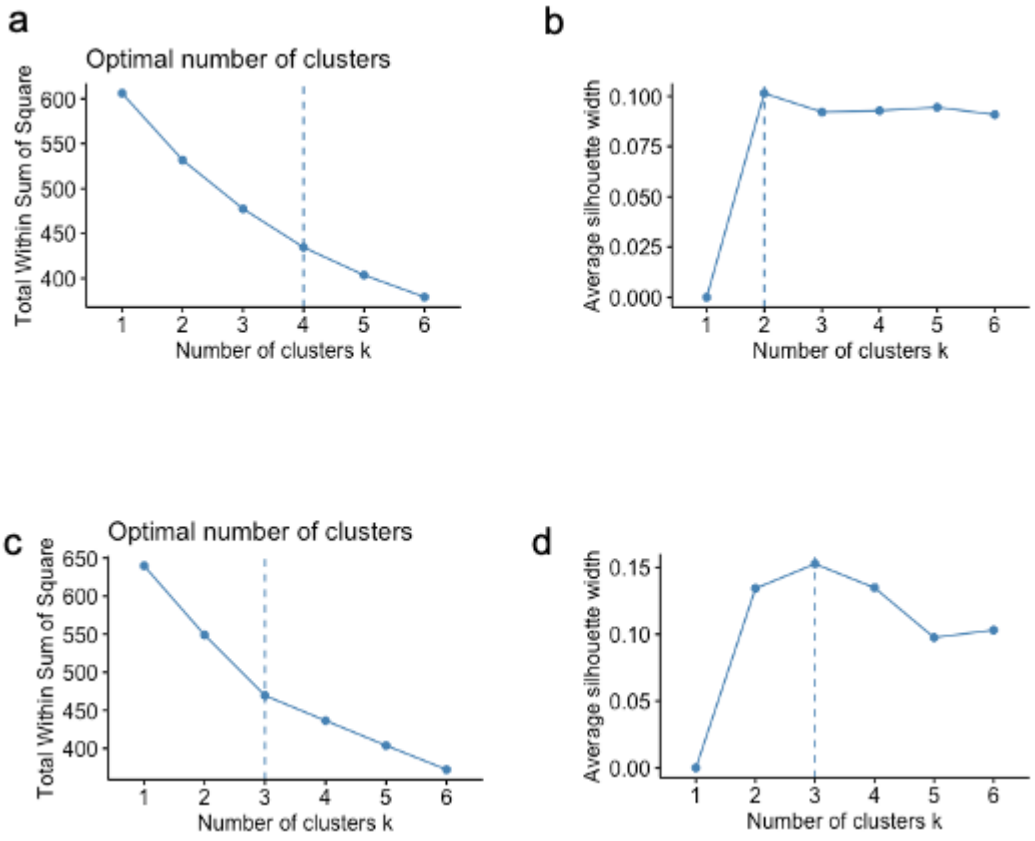

**Figure S2 Amygdala reactivity to threat after traumas producing different levels of injury severity.** Greater injury severity was linked with greater amygdala reactivity to threat, $F_{1,144}=4.58$, $p=0.03$.

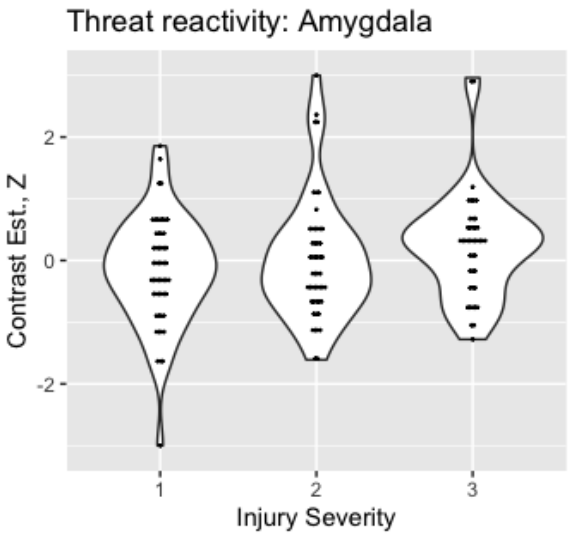

**Figure S3. Sitewise differences in quality assurance metrics.** Differences in framewise displacement (FD), standard deviation in the global signal (DVARs), and temporal signal-to-noise ratio (TSNR) were calculated between each neuroimaging site. Black bars reflect the mean value of each metric per site, and dots illustrate each participant of the combined n=146 (discovery + replication cohorts).

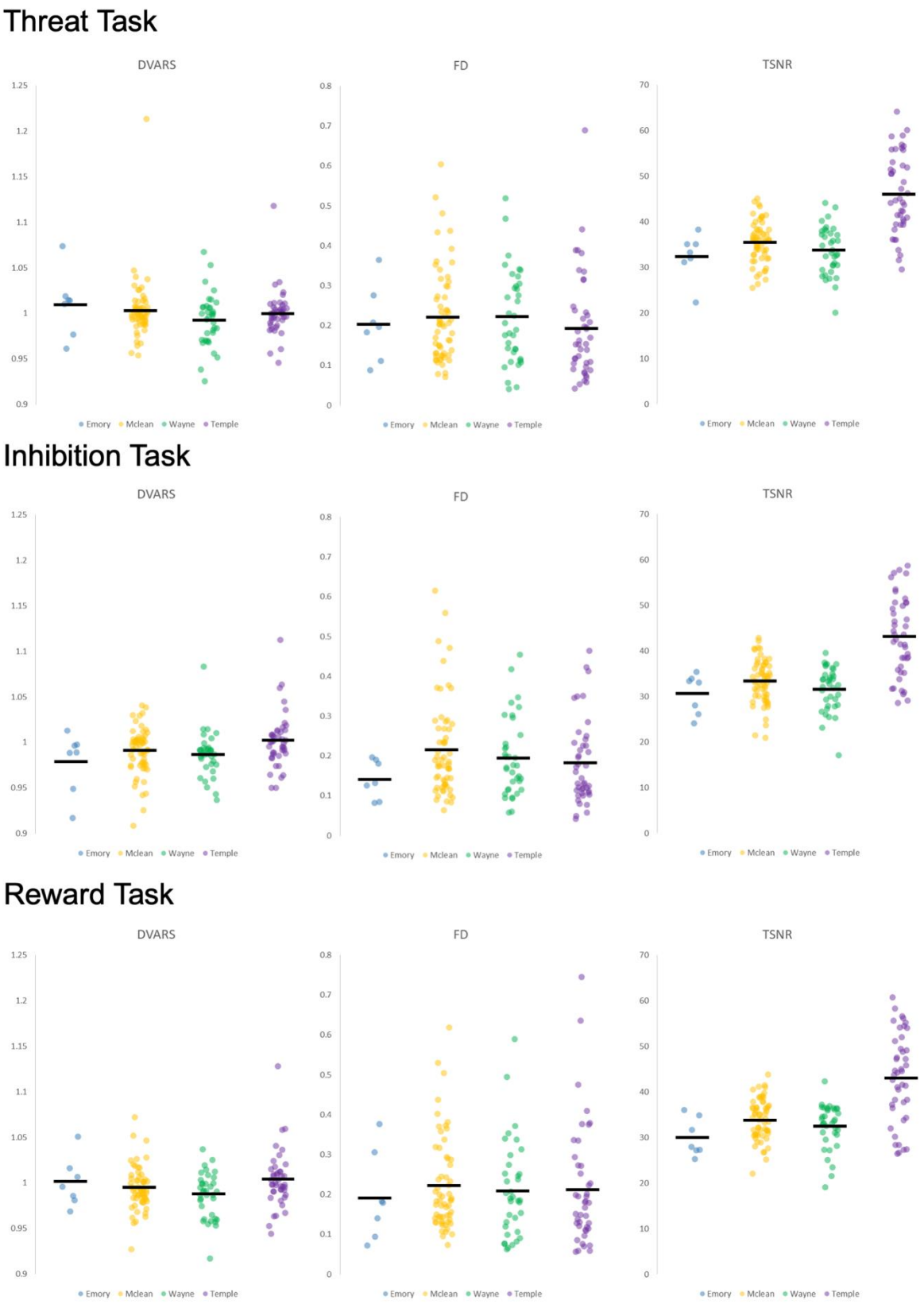

**References**


Abraham A, Pedregosa F, Eickenberg M, Gervais P, Mueller A, Kossaifi J, Gramfort A, Thirion B, Varoquaux G. Machine learning for neuroimaging with scikit-learn. Front in Neuroinf 8:14. 2014. doi:10.3389/fninf.2014.00014.

Andersson, J L R, Jenkinson, M., & Smith, S. (2007). Non-linear registration aka spatial normalisation. FMRIB Technical Report TRO7JA2. Retrieved from http://fmrib.medsci.ox.ac.uk/analysis/techrep/tr07ja2/tr07ja2.pdf

Andersson, Jesper L.R., & Sotiropoulos, S. N. (2016). An integrated approach to correction for off-resonance effects and subject movement in diffusion MR imaging. NeuroImage, 125, 1063–1078. https://doi.org/10.1016/j.neuroimage.2015.10.019

Avants BB, Epstein CL, Grossman M, Gee JC. Symmetric diffeomorphic image registration with cross-correlation: evaluating automated labeling of elderly and neurodegenerative brain. Med Image Anal. 2008 Feb;12(1):26–41. doi:10.1016/j.media.2007.06.004.

Behzadi Y, Restom K, Liau J, Liu TT. A component based noise correction method (CompCor) for BOLD and perfusion based fMRI. Neuroimage. 2007 Aug 1;37(1):90–101. doi:10.1016/j.neuroimage.2007.04.042.

Bernstein, D. P., & Fink, L. (1998). Childhood trauma questionnaire: A retrospective self-report: Manual: Psychological Corporation.

Carlson, E. B., & Putnam, F. W. (1993). An update on the dissociative experiences scale. Dissociation: progress in the dissociative disorders.

Cox RW. AFNI: software for analysis and visualization of functional magnetic resonance neuroimages. Comput Biomed Res. 1996 Jun;29(3):162–73. doi:10.1006/cbmr.1996.0014.

Cyders, M.A., Littlefield, A.K., Coffey, S., Karyadi, K.A. (2014). Examination of a short English version of the UPPS-P Impulsive Behavior Scale. Addictive Behaviors, 39(9), 1372-1376.

Dale A, Fischl B, Sereno MI. Cortical Surface-Based Analysis: I. Segmentation and Surface Reconstruction. Neuroimage. 1999;9(2):179–94. doi:10.1006/nimg.1998.0395.

Esteban O, Birman D, Schaer M, Koyejo OO, Poldrack RA, Gorgolewski KJ; MRIQC: Advancing the Automatic Prediction of Image Quality in MRI from Unseen Sites; PLOS ONE. September 2017; 12(9):e0184661; doi:10.1371/journal.pone.0184661.

Esteban, O., Blair, R., Markiewicz, C. J., Berleant, S. L., Moodie, C., Ma, F., ... & Poldrack, R. A. poldracklab/fmriprep: 1.0. 0-rc10, November 2017. URL https://doi. org/ 10.5281/zenodo.852659.

Esteban O, Markiewicz CJ, Blair RW, Moodie CA, Isik AI, Erramuzpe A, Kent JD, Goncalves M, DuPre E, Snyder M, Oya H, Ghosh SS, Wright J, Durnez J, Poldrack RA, Gorgolewski KJ. fMRIPrep: a robust preprocessing pipeline for functional MRI. Nat Meth. 2018; doi:10.1038/s41592-018-0235-4

Fischl, B., Van Der Kouwe, A., Destrieux, C., Halgren, E., Ségonne, F., Salat, D. H., . . . Kennedy, D. (2004). Automatically parcellating the human cerebral cortex. Cerebral Cortex, 14(1), 11-22.

Fonov VS, Evans AC, McKinstry RC, Almli CR, Collins DL. Unbiased nonlinear average age-appropriate brain templates from birth to adulthood. NeuroImage; Amsterdam. 2009 Jul 1;47:S102. doi:10.1016/S1053-8119(09)70884-5.

Gennarelli, T. A., & Wodzin, E. (2006). AIS 2005: a contemporary injury scale. Injury, 37(12), 1083-1091. doi:10.1016/j.injury.2006.07.009

Glover, E. M., Jovanovic, T., Mercer, K. B., Kerley, K., Bradley, B., Ressler, K. J., & Norrholm, S. D. (2012). Estrogen levels are associated with extinction deficits in women with posttraumatic stress disorder. Biol Psychiatry, 72(1), 19-24. doi:10.1016/j.biopsych.2012.02.031

Gorgolewski K, Burns CD, Madison C, Clark D, Halchenko YO, Waskom ML, Ghosh SS. Nipype: a flexible, lightweight and extensible neuroimaging data processing framework in python. Front Neuroinform. 2011 Aug 22;5(August):13. doi:10.3389/fninf.2011.00013.

Gorgolewski KJ, Esteban O, Ellis DG, Notter MP, Ziegler E, Johnson H, Hamalainen C, Yvernault B, Burns C, Manhães-Savio A, Jarecka D, Markiewicz CJ, Salo T, Clark D, Waskom M, Wong J, Modat M, Dewey BE, Clark MG, Dayan M, Loney F, Madison C, Gramfort A, Keshavan A, Berleant S, Pinsard B, Goncalves M, Clark D, Cipollini B, Varoquaux G, Wassermann D, Rokem A, Halchenko YO, Forbes J, Moloney B, Malone IB, Hanke M, Mordom D, Buchanan C, Pauli WM, Huntenburg JM, Horea C, Schwartz Y, Tungaraza R, Iqbal S, Kleesiek J, Sikka S, Frohlich C, Kent J, Perez-Guevara M, Watanabe

A, Welch D, Cumba C, Ginsburg D, Eshaghi A, Kastman E, Bougacha S, Blair R, Acland B, Gillman A, Schaefer A, Nichols BN, Giavasis S, Erickson D, Correa C, Ghayoor A, Küttner R, Haselgrove C, Zhou D, Craddock RC, Haehn D, Lampe L, Millman J, Lai J, Renfro M, Liu S, Stadler J, Glatard T, Kahn AE, Kong X-Z, Triplett W, Park A, McDermottroe C, Hallquist M, Poldrack R, Perkins LN, Noel M, Gerhard S, Salvatore J, Mertz F, Broderick W, Inati S, Hinds O, Brett M, Durnez J, Tambini A, Rothmei S, Andberg SK, Cooper G, Marina A, Mattfeld A, Urchs S, Sharp P, Matsubara K, Geisler D, Cheung B, Floren A, Nickson T, Pannetier N, Weinstein A, Dubois M, Arias J, Tarbert C, Schlamp K, Jordan K, Liem F, Saase V, Harms R, Khanuja R, Podranski K, Flandin G, Papadopoulos Orfanos D, Schwabacher I, McNamee D, Falkiewicz M, Pellman J, Linkersdörfer J, Varada J, Pérez-García F, Davison A, Shachnev D, Ghosh S. Nipype: a flexible, lightweight and extensible neuroimaging data processing framework in Python. 2017. doi:10.5281/zenodo.581704.

Greve DN, Fischl B. Accurate and robust brain image alignment using boundary-based registration. Neuroimage. 2009 Oct;48(1):63–72. doi:10.1016/j.neuroimage.2009.06.060.

Hammers, A., Allom, R., Koepp, M. J., Free, S. L., Myers, R., Lemieux, L., . . . Duncan, J. S. (2003). Three-dimensional maximum probability atlas of the human brain, with particular reference to the temporal lobe. Human Brain Mapping, 19(4), 224-247. Retrieved from https://onlinelibrary.wiley.com/doi/full/10.1002/hbm.10123

Iglesias, J. E., Liu, C. Y., Thompson, P. M., & Tu, Z. (2011). Robust brain extraction across datasets and comparison with publicly available methods. IEEE Transactions on Medical Imaging, 30(9), 1617–1634. https://doi.org/10.1109/TMI.2011.2138152

Jenkinson M, Bannister P, Brady M, Smith S. Improved optimization for the robust and accurate linear registration and motion correction of brain images. Neuroimage. 2002 Oct;17(2):825–41. doi:10.1006/nimg.2002.1132.

Jovanovic, T., Blanding, N. Q., Norrholm, S. D., Duncan, E., Bradley, B., & Ressler, K. J. (2009). Childhood abuse is associated with increased startle reactivity in adulthood. Depress Anxiety, 26(11), 1018-1026. doi:10.1002/da.20599

Jovanovic, T., Ely, T., Fani, N., Glover, E. M., Gutman, D., Tone, E. B., . . . Ressler, K. J. (2013). Reduced neural activation during an inhibition task is associated with impaired fear inhibition in a traumatized civilian sample. Cortex, 49(7), 1884-1891. doi:10.1016/j.cortex.2012.08.011

Klein A, Ghosh SS, Bao FS, Giard J, Häme Y, Stavsky E, et al. Mindboggling morphometry of human brains. PLoS Comput Biol 13(2): e1005350. 2017. doi:10.1371/journal.pcbi.1005350.

Lanczos, C. (1964). Evaluation of noisy data. Journal of the Society for Industrial and Applied Mathematics, Series B: Numerical Analysis, 1(1), 76-85.

Leon, A. C., Olfson, M., Portera, L., Farber, L., & Sheehan, D. V. (1997). Assessing psychiatric impairment in primary care with the Sheehan Disability Scale. The international journal of psychiatry in medicine, 27(2), 93-105. Retrieved from https://journals.sagepub.com/doi/abs/10.2190/T8EM-C8YH-373N-1UWD

Li X, Morgan PS, Ashburner J, Smith J, Rorden C (2016) The first step for neuroimaging data analysis: DICOM to NIfTI conversion. J Neurosci Methods. 264:47-56. doi: 10.1016/j.jneumeth.2016.03.001. PMID: 26945974

Orben, A., & Lakens, D. Crud (Re)Defined. Advances in Methods and Practices in Psychological Science, 0(0), 2515245920917961. doi:10.1177/2515245920917961

Pauli, W. M., Nili, A. N., & Tyszka, J. M. (2018). A high-resolution probabilistic in vivo atlas of human subcortical brain nuclei. Scientific data, 5, 180063.

Pilkonis, P. A., Choi, S. W., Reise, S. P., Stover, A. M., Riley, W. T., Cella, D., & Group, P. C. (2011). Item banks for measuring emotional distress from the Patient-Reported Outcomes Measurement Information System (PROMIS®): depression, anxiety, and anger. Assessment, 18(3), 263-283.

Power JD, Mitra A, Laumann TO, Snyder AZ, Schlaggar BL, Petersen SE. Methods to detect, characterize, and remove motion artifact in resting state fMRI. Neuroimage. 2013 Aug 29;84:320–41. doi:10.1016/j.neuroimage.2013.08.048.

Pruim RHR, Mennes M, van Rooij D, Llera A, Buitelaar JK, Beckmann CF. ICA-AROMA: A robust ICA-based strategy for removing motion artifacts from fMRI data. Neuroimage. 2015 May 15;112:267–77. doi:10.1016/j.neuroimage.2015.02.064.

Roalf, D. R., Quarmley, M., Elliott, M. A., Satterthwaite, T. D., Vandekar, S. N., Ruparel, K., ... & Prabhakaran, K. (2016). The impact of quality assurance assessment on diffusion tensor imaging outcomes in a large-scale population-based cohort. Neuroimage, 125, 903-919.

Satterthwaite, T. D., Ciric, R., Roalf, D. R., Davatzikos, C., Bassett, D. S., & Wolf, D. H. (2019). Motion artifact in studies of functional connectivity: Characteristics and mitigation strategies. Human Brain Mapping, 40(7), 2033-2051. Retrieved from https://www.ncbi.nlm.nih.gov/pmc/articles/PMC5930165/pdf/nihms878475.pdf

Sheehan, D. V., Harnett-Sheehan, K., & Raj, B. A. (1996). The measurement of disability. Int Clin Psychopharmacol, 11 Suppl 3, 89-95. doi:10.1097/00004850-199606003-00015

Smith, S. M., Jenkinson, M., Woolrich, M. W., Beckmann, C. F., Behrens, T. E. J., Johansen-Berg, H., … Matthews, P. M. (2004). Advances in functional and structural MR image analysis and implementation as FSL. In NeuroImage (Vol. 23). https://doi.org/10.1016/j.neuroimage.2004.07.051

Tang, W., Jbabdi, S., Zhu, Z., Cottaar, M., Grisot, G., Lehman, J. F., . . . Haber, S. N. (2019). A connectional hub in the rostral anterior cingulate cortex links areas of emotion and cognitive control. eLife, 8, e43761. doi:10.7554/eLife.43761

Tustison NJ, Avants BB, Cook PA, Zheng Y, Egan A, Yushkevich PA, Gee JC. N4ITK: improved N3 bias correction. IEEE Trans Med Imaging. 2010 Jun;29(6):1310–20. doi:10.1109/TMI.2010.2046908.

Tyszka, J. M., & Pauli, W. M. (2016). In vivo delineation of subdivisions of the human amygdaloid complex in a high-resolution group template. Human Brain Mapping, 37(11), 3979-3998.

Tzourio-Mazoyer, N., Landeau, B., Papathanassiou, D., Crivello, F., Etard, O., Delcroix, N., . . . Joliot, M. (2002). Automated anatomical labeling of activations in SPM using a macroscopic anatomical parcellation of the MNI MRI single-subject brain. Neuroimage, 15(1), 273-289. Retrieved from http://www.sciencedirect.com/science/article/B6WNP-4575RNN-1F/2/3d7eadc4477a1a64629325332495df1d

Wang, S., Peterson, D. J., Gatenby, J. C., Li, W., Grabowski, T. J., & Madhyastha, T. M. (2017). Evaluation of field map and nonlinear registration methods for correction of susceptibility artifacts in diffusion MRI. Frontiers in Neuroinformatics, 11. https://doi.org/10.3389/fninf.2017.00017

Ware Jr, J. E., Kosinski, M., & Keller, S. D. (1996). A 12-Item Short-Form Health Survey: construction of scales and preliminary tests of reliability and validity. Medical care, 220-233.

Weathers, F. W., Litz, B. T., Keane, T. M., Palmieri, P. A., Marx, B. P., & Schnurr, P. P. (2013). The PTSD Checklist for DSM-5 (PCL-5). Scale available from the National Center for PTSD at www. ptsd. va. gov, 10.

Zhang Y, Brady M, Smith S. Segmentation of brain MR images through a hidden Markov random field model and the expectation-maximization algorithm. IEEE Trans Med Imaging. 2001 Jan;20(1):45–57. doi:10.1109/42.906424.